energies

MDPI

Article

Thermodynamic, Exergoeconomic and Multi-Objective Analyses of Supercritical N_2O-He Recompression Brayton Cycle for a Nuclear Spacecraft Application

Xinyu Miao [1], Haochun Zhang [1,*], Qi Wang [1], Wenbo Sun [1] and Yan Xia [2]

[1] School of Energy Science and Engineering, Harbin Institute of Technology, Harbin 150001, China
[2] Institute of Spacecraft System Engineering, China Academy of Space Technology, Beijing 100081, China
* Correspondence: hczhang@hit.edu.cn; Tel.: +86-189-4504-5111

Abstract: Detailed thermodynamic, exergoeconomic, and multi-objective analysis are performed for a supercritical recompression Brayton cycle in which the advanced working medium mixture of nitrous oxide and helium (N_2O–He) is utilized for power generation. The thermodynamic and exergoeconomic models are propitious based on the standard components' mass and energy conservation, exergy balance equation, and exergy cost calculation equation. An investigation of the sensitivity parametric is considered for judging the impact of crucial decision variable parameters on the performance of the proposed Brayton cycle. The proposed cycle's performance is evaluated by systematic analysis of the thermal efficiency (η_{th}), exergy efficiency (η_{ex}), total cost rate ($\dot{C}_{total}$), levelized cost of electricity (*LCOE*), and the total heat transfer area (A_{total}). Furthermore, multi-objective optimization is adopted from the viewpoint of the first and second laws of exergoeconomics to find the optimum operating parameters and to improve the circular's exergoeconomic performance. The final results illustrate that the optimization calculation is based on the fact of the exergoeconomics method; the whole system produces electrical power of 0.277 MW with $\dot{C}_{total}$ of USD 18.37/h, while the η_{th}, η_{ex}, A_{total}, and *LCOE* are 49.14%, 67.29%, 165.55 m^2 and USD 0.0196/kWh, respectively. It is concluded that the work exergy destruction for the reactor and turbine is higher than that of other components; then, after the multi-objective optimization analysis, the η_{th} and η_{ex} improved by 2.08% and 5.07%, respectively, and the $\dot{C}_{total}$, A_{total}, and *LCOE* decreased by 13.99%, 0.01%, and 5.13%, respectively.

Keywords: recompression Brayton cycle; supercritical N_2O-He; exergy analysis; sensitivity analysis; exergoeconomic; multi-objective optimization

Citation: Miao, X.; Zhang, H.; Wang, Q.; Sun, W.; Xia, Y. Thermodynamic, Exergoeconomic and Multi-Objective Analyses of Supercritical N_2O-He Recompression Brayton Cycle for a Nuclear Spacecraft Application. *Energies* **2022**, *15*, 8184. https://doi.org/10.3390/en15218184

Academic Editor: Alessandro Cannavale

Received: 8 October 2022
Accepted: 31 October 2022
Published: 2 November 2022

1. Introduction

Concerns over restrictions of mass, mission time, and long-distance interstellar flight suggest an essential role for the nuclear electric propulsion (NEP) system in future deep space, even extrasolar exploration. The NEP system is simple electric propulsion in which the electricity is derived from a nuclear reactor. The thrusting fluid (gas, ion, plasma) receives its energy to accelerate from the application of electric fields, either directly heating the gas as in an arc jet, using an electric field to accelerate ions, or a magnetic field as in the magnetoplasmadynamic (MPD) approach. In order to successfully utilize nuclear power, many studies have been carried out to improve thermoelectric conversion efficiency, be lightweight, and reduce the power generation cost of spacecraft. High-efficiency thermoelectric conversion devices include static and dynamic conversion methods [1].

Static methods:

- Thermocouple conversion system;
- Thermionic conversion system.

Dynamic methods:

- Brayton conversion system;

- Rankine conversion system;
- Stirling conversion system.

The Brayton cycle has higher thermoelectric conversion efficiency than other conversion methods. It can convert approximately 20% to 35% of the whole thermal energy transported by the reactor part into electrical energy through dynamic mechanical processes [2]. Recently, the recompression Brayton cycle power generation has become a research frontier due to its advantages of compact and higher thermal efficiency [3] with a simple structure [4]. The recompression Brayton cycle is shown in Figure 1. To select suitable supercritical cycle structures, a lot of research was carried out during the period, with over 40 structures studied [5]. In 2015, Sulaiman's research found that a system with a re-compressor has advanced performance compared to the simple system, regeneration system, pre-compression system, partial cooling system, segmented expansion system, and other structures [6]. The cycle with a re-compressor can weaken the influence of the "pinch point" of the cycle that may occur in the recuperator and regenerator, and the supercritical cycle is found to be more efficacious [7,8].

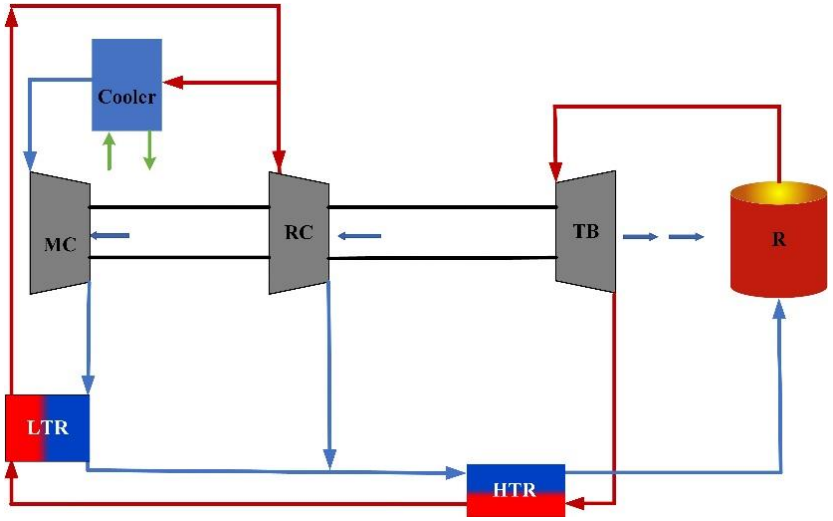

Figure 1. Diagram for the recompression Brayton cycle.

For the supercritical Brayton cycle, Sarkar [9] studied the exergy and optimization of the cycle and investigated the influence of pressure ratio, cycle energy, and thermal efficiency. Sarkar and Bhattacharyya [10] optimized the supercritical recompression Brayton cycle, achieving the maximum efficiency and the thermal efficiency improved by 3.5% when used reheating. Wang et al. [11] adopted the genetic algorithm (GA) method for the optimization of cycle parameters to obtain the maximum efficiency (thermal efficiency and exergy efficiency). P. Serrano et al. [12] designed a new arrangement scheme in which a bypass low-temperature cladding source replaced one of the regenerators. In the new arrangement scheme, high system efficiency can be achieved at the high inlet temperature of the turbine with medium pressures.

A revolutionary supercritical working medium, nitrous oxide and helium (N_2O–He), was performed for the proposed recompression Brayton cycle [13] to convert thermal energy into electricity. In the N_2O–He mixture's components, the N_2O part has thermodynamic properties such as molecular weight, critical pressure, and temperature, causing almost comparable behaviors under operating conditions that may improve the N_2O system's performance and can use the existing CO_2 configuration. Sarkar J. [14] utilized supercritical N_2O (S-N_2O) as the working medium to combine the Brayton cycle with the new generation nuclear reactors. Its thermal efficiency is higher than that of the S-CO_2 system. Characteristics of several critical working fluids at the critical point are shown in Table 1. Using these mixtures (CO_2-He [15], CO_2-C_2H_6/SF_6 [16], binary mixture [17]) can further

improve the thermodynamic cycling performance of different Brayton cycles. The mixed working medium Brayton cycle research has apparent advantages over the pure S-CO_2 Brayton cycle.

Table 1. Physical properties of the working medium at critical point [18].

Name	Molecular Formula	Critical Temperature (K)	Critical Pressure (MPa)	Critical Density (kg/m^3)
Carbon Dioxide	CO_2	304.05	7.38	467.6
Ethane	C_2H_6	305.35	4.87	206.2
Nitrous Oxide	N_2O	309.55	7.24	452.0
Sulfur Hexafluoride	SF_6	318.75	3.75	724.3.
Water	H_2O	647.05	22.13	322.0

The research mentioned above is devoted primarily to thermodynamic analysis, and we know that comprehensive exergoeconomic analyses work on the recompression supercritical N_2O–He mixture Brayton cycle has not been reported yet. Moreover, some literature merely concerns the exergoeconomic analyses of the S-CO_2 Brayton system. A detailed exergoeconomic investigation and thermoeconomic analysis needs to also be conducted.

In this study, energy, exergy, and exergoeconomic theory of the recompression Brayton cycle are analyzed using the novelty working medium N_2O-He mixture with the mole fractions of N_2O and He of 85% and 15% (85%N_2O–15%He). Firstly, comprehensive energy and exergy studies are analyzed, and the exergy cost theory is applied to the cycle. Moreover, a parameter sensitivity analysis is presented to reveal the influence of the proposed cycle on the thermal and exergy efficiency and total cost of the nuclear-powered spacecraft. Finally, from the perspective of exergoeconomics, the supercritical N_2O–He Brayton cycle is optimized, and the appropriate parameters of various components' thermal efficiency (η_{th}), exergy efficiency (η_{ex}), total cost rate ($\dot{C}_{total}$), total heat transfer area (A_{total}), and levelized cost of electricity (*LCOE*) are selected by the GA method.

2. System Description and Assumptions

An NEP system with a typical Brayton cycle unit can be separated into six subsystems, depicted in Figure 2. The NEP system's six subsystems are the reactor core, shielding, power conversion unit, heat dissipation, power management and distribution (PMAD), and electric propulsion (EP). The supercritical 85%N_2O–15%He recompression Brayton conversion unit consists of a heat source reactor (R), a TB (turbine), an MC (main compressor), an RC (recompression compressor), a G (generator), an HTR (high temperature recuperator), an LTR (low temperature recuperator), a cooler, and a radiator. The recompression Brayton cycle schematic diagram is presented in Figure 3. The T-s diagram for the proposed corresponding S-(N_2O-He) recompression Brayton cycle is shown in Figure 4.

The supercritical N_2O-He stream leaving the high temperature reactor enters the TB as a working fluid (1–2), where it expands and produces power (2–3). Then, the expansion flow successfully flows through the HTR and LTR to heat the recompression flow (3–4–5). The air flows out of the LTR and is split into two streams (state 5). One stream,5a, has a high mass flow rate, and the other stream, 5b, has a low mass flow rate. The partial flow of 5a is cooled in the cooler component (5a–6) and then compressed in the MC to higher pressure (6–7). The stream flowing out of the MC absorbs heat from the LTR (7–8a) and is mixed with the steam, which is compressed by RC to the same pressure as MC (5b–8b). The two partial split streams are mixed at state point 8 and then enter into the HTR and are heated before flowing into the reactor core part (8–1). In this way, a complete thermodynamic cycle is formed.

The space nuclear reactor system of the actual recompression Brayton cycle includes the nuclear reactor core, high temperature recuperator, low temperature recuperator, heat accumulators, panel-type radiation radiators, turbine machinery, main compressor and

re-compressor machinery, heat pipe and other complex and auxiliary equipment. The equipment structure is complex in the actual operation, and the operating condition is variable, so the system needs to be simplified. After the system is simplified, the cycle process can be better modeled to explore its cycle performance.

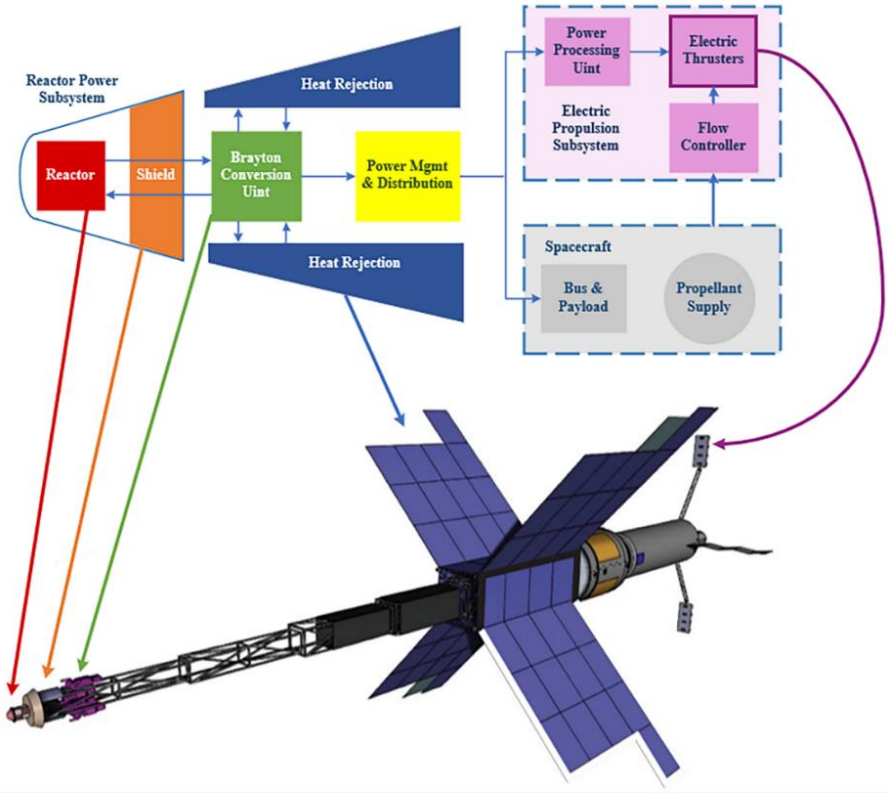

Figure 2. NEP subsystems and conceptual design.

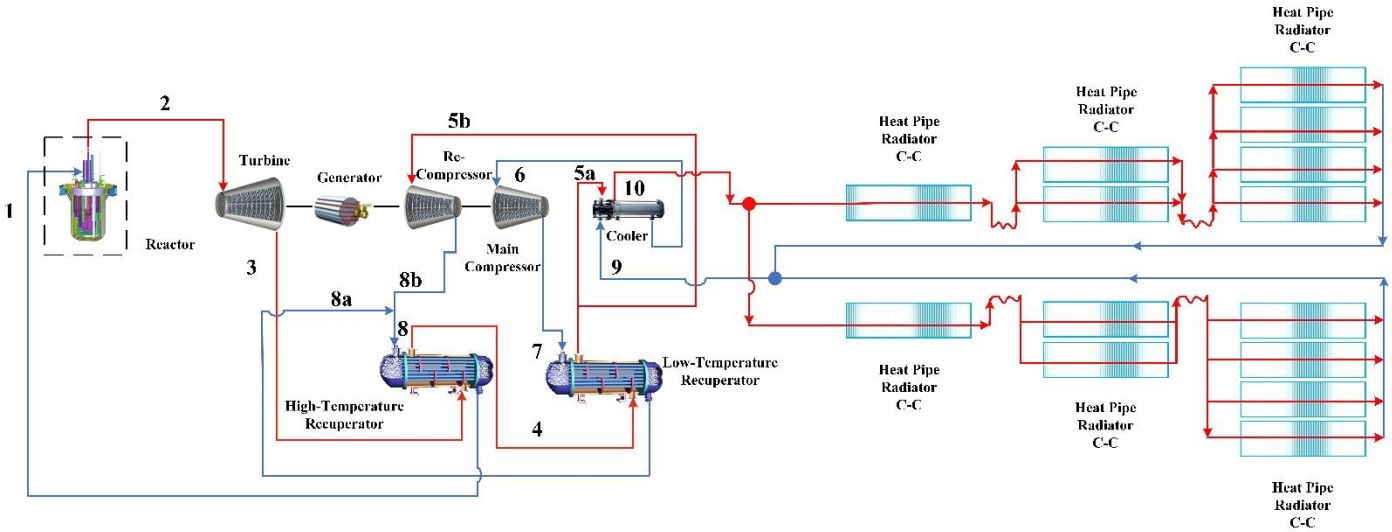

Figure 3. Structure diagram for the proposed S-(N_2O-He) cycle.

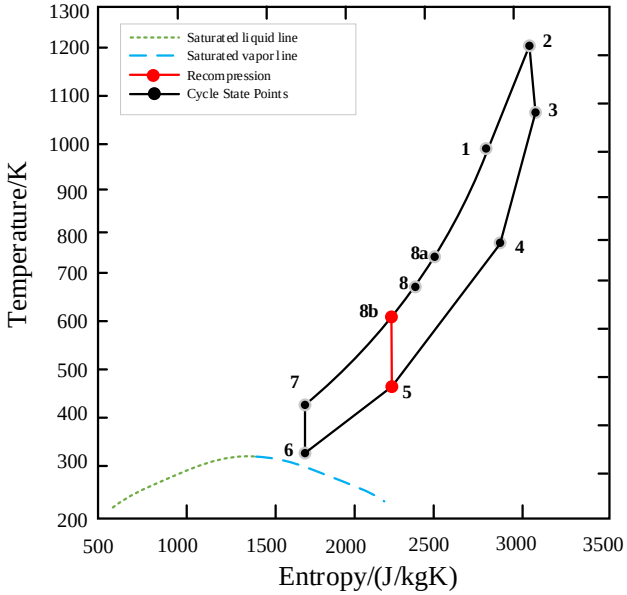

Figure 4. T-s diagram representation for the proposed S-(N_2O-He) cycle [13].

The study of this paper is conducted on the general assumptions as below:

- All processes reach the stable state.
- Turbine and compressor processes are adiabatic.
- The pressure loss of the heat exchanger is negligible.
- Kinetic energy and potential energy and heat transfer to the environment of the system are neglected.
- The efficiency of the turbine (TB) and compressors (MC and RC) is isentropic efficiencies.
- The effectiveness of the HTR and the LTR is considered.

According to the above assumptions, the actual recompressed Brayton cycle space nuclear energy system is simplified to the recompressed closed Brayton cycle system, which becomes the most basic thermal cycle process composition.

3. Methods and Model Design

3.1. Thermodynamic Analysis

This work extends previous research [13,19], particularly concerning each state point's thermodynamic and exergy analysis. Table 2 lists calculation equations for each component's energy, exergy, and mass balance.

Table 2. Range of the decision operating parameters.

Parameter	Range
Split ratio—x	0.25–0.4
Pressure ratio—π	2.5–3.5
MC inlet temperature—T_6	315–340 K
TB inlet temperature—T_2	1000–1200 K
MC inlet pressure—P_6	7.4–8.4 MPa

The study of the Brayton cycle is based on the theory of mass, energy, and exergy equilibrium, which is shown as follows:

$$\sum \dot{m}_i = \sum \dot{m}_e \tag{1}$$

$$\dot{Q} - \dot{W} = \sum \dot{m}_e h_e - \sum \dot{m}_i h_i \tag{2}$$

$$\dot{E}_Q + \sum \dot{E}_i = \dot{E}_W + \sum \dot{E}_e + \dot{E}_{De} \tag{3}$$

where subscript i represents the value of the entry state point, and e represents the value of the exit state point. $\dot{E}_{De}$ is the exergy destruction rate in the component.

Stream exergy consists of four main parts, which are $\dot{E}_{ph}$ (stream physical exergy), $\dot{E}_{ch}$ (stream chemical exergy), $\dot{E}_k$ (stream kinetic exergy), and $\dot{E}_p$ (stream potential exergy). Regardless of the $\dot{E}_k$ and $\dot{E}_p$ of the working medium, total exergy of the working medium $\dot{E}_{total}$ is modified as follows [20]:

$$\dot{E}_{total} = \dot{E}_{ph} + \dot{E}_{ch} \tag{4}$$

In the work at this stage, there is a chemical reaction process of the working medium in the cycle, and the working fluid passes through different system components, so only consider the working medium's physical exergy. The calculation formula can be defined as [20]:

$$\dot{E}_{ph} = \dot{m} \times [(h - h_0) - T_0(s - s_0)] \tag{5}$$

In the equation, the subscript "0" indicates the value of environmental conditions. T_0 is space environment temperature. The environmental conditions for the proposed cycle are T_0 = 298 K and P_0 = 0.101 MPa.

The effectiveness for each recuperator is defined and can be estimated as [19].

$$\varepsilon_{HTR} = \frac{T_3 - T_4}{T_3 - T_8} \tag{6}$$

$$\varepsilon_{LTR} = \frac{T_4 - T_5}{T_4 - T_7} \tag{7}$$

The thermodynamic model for the HTR and the LTR are given by [21]:

$$h_3 - h_4 = h_1 - h_8 \tag{8}$$

$$\dot{m}_4(h_{8a} - h_7) = \dot{m}_7(h_4 - h_5) \tag{9}$$

The efficiency expressions for the TB, MC, and RC can be calculated by [14]:

$$\eta_{TB} = \frac{h_2 - h_3}{h_2 - h_{3s}} \tag{10}$$

$$\eta_{MC} = \frac{h_{7s} - h_6}{h_7 - h_6} \tag{11}$$

$$\eta_{RC} = \frac{h_{8s} - h_5}{h_8 - h_5} \tag{12}$$

The subscript "s" is the isentropic process.

The thermodynamic calculation relations of the TB, MC, and RC are as follows [14]:

$$\dot{W}_{TB} = \dot{m}_2(h_3 - h_2) \tag{13}$$

$$\dot{W}_{MC} = \dot{m}_7(h_7 - h_6) \tag{14}$$

$$\dot{W}_{RC} = \dot{m}_{5b}(h_8 - h_5) \tag{15}$$

Specific heat input of the reactor ($\dot{Q}_R$) is expressed as:

$$\dot{Q}_R = \dot{m}_1(h_2 - h_1) \tag{16}$$

The net power of circulating, W_{net}, is defined as:

$$\dot{W}_{net} = \dot{W}_{TB} - \left(\dot{W}_{MC} + \dot{W}_{RC}\right) \tag{17}$$

The system thermal efficiency can be calculated by:

$$\eta_{th} = \frac{\dot{W}_{net}}{\dot{Q}_R} \tag{18}$$

The system exergy efficiency is calculated by:

$$\eta_{ex} = \frac{\dot{W}_{net}}{\dot{E}_{in}} = \frac{\dot{W}_{net}}{\dot{Q}_R(1 - T_0/T_R)} \tag{19}$$

where $\dot{E}_{in}$ is the exergy entering the reactor, and T_R is the reactor temperature.

The details of the relations for energy and exergy balance equations for each component are provided in Appendix A. Energy and exergy balance calculation equations are listed in Table A1.

3.2. Exergoeconomic Analysis

A cost-effective energy conversion system is vital for the cycle, so economic consideration should be considered. Exergoeconomic analysis needs to consider the theory of the exergy cost [22], the average cost analysis method [23], specific exergy cost calculation [24–26], and basic economic theory principles. The purpose of exergy economic analysis is to study and calculate the exergy cost of unit product flow by revealing the system's cost formation process. For system components that receive thermal energy and generate electricity, the equation of cost balance can be expressed as follows [27]:

$$\sum \dot{C}_{out,j} + \dot{C}_{W,j} = \sum \dot{C}_{in,j} + \dot{C}_{Q,j} + \dot{Z}_j \tag{20}$$

In Equation (20), $\dot{C}_{Q,j}$ is the cost rate related to component input heat, and $\dot{C}_{W,j}$ is the cost rate of component output power. It can be seen from Equation (20) that the total cost rate of working medium exiting exergy is the sum of the total cost rate of working medium entering exergy and the total cost expenditure rate.

The calculation formula of the unit exergy cost rate is as follows [28]:

$$\dot{C}_j = c_j \times \dot{E}_j \tag{21}$$

$$\dot{C}_W = c_W \times \dot{E}_W \tag{22}$$

$$\dot{C}_Q = c_Q \times \dot{E}_Q \tag{23}$$

In Equations (21)–(23), c_j, c_W, and c_Q are the per unit of cost exergy, \$/GJ.

$\dot{Z}_j$ in calculation Formula (20) is the total cost rate related to the capital investment (CI) cost and operation and maintenance (OM) cost of the jth system component [20]:

$$\dot{Z}_j = \dot{Z}_j^{CI} + \dot{Z}_j^{OM} \tag{24}$$

The component j's annual levelized CI can be calculated by [27,29]:

$$\dot{Z}_j^{CI} = (\frac{CRF}{\tau}) \times Z_j \tag{25}$$

In Equation (25), the CRF represents the capital recovery factor, and τ is the service life of the power system.

The annual leveling of the OM cost is calculated according to [27]:

$$\dot{Z}_j^{OM} = (\frac{\gamma_j}{\tau}) \times Z_j \tag{26}$$

Table 3 lists the factors CRF, τ, γ_k, and Z_j of the system's different components.

We update the Chemical Engineering Plant Cost Index (*CEPCI*) of equipment costs to 2021 values.

$$Z_{2021} = Z_{original} \times \frac{CEPCI_{2021}}{CEPCI_{original}} \tag{27}$$

where $CEPCI_{2021}$ = 596.2 [30], and $Z_{original}$ is each component's original cost. The Z_k calculation details for each component of the proposed cycle are listed in Appendix B.

The cost balance for the different components of the proposed cycle and the auxiliary equations required are all presented in Table A2. The Gauss–Seidel method is used to solve the various linear equations in Table A3. As shown in Table A4, several essential indicators are used to identify economic behavior. The total cost rate ($\dot{C}_{total}$) is given in Table A4, which is the sum of these values, including the CI cost rate, the total exergy destruction cost rate ($\dot{C}_D$), and the OM cost rate.

3.3. Performance Evaluation Index of the Cycle

$\dot{W}_{net}$, η_{th}, η_{ex}, $\dot{C}_{total}$, A_{total}, and *LOCE* are the evaluation metric for improving the operating system performance.

- Net power ($\dot{W}_{net}$) is shown as Equation (17).
- Thermal efficiency (η_{th}) is calculated by Equation (18).
- Exergy efficiency (η_{ex}) can be calculated by Equation (19).
- Total cost rate ($\dot{C}_{total}$) is calculated by the equation in Table A4.
- The price of electricity can be estimated using the levelized cost of electricity (*LCOE*) parameter. It is given as [31]:

$$LCOE = \frac{\dot{Z}_{total}}{\dot{W}_{net}} \left(\frac{\$}{\mathrm{kW \cdot h}}\right) \tag{28}$$

3.4. Parameter Selection of Sensitivity Analysis

The parameter selection of sensitivity analysis aims to analyze the influence of various working conditions and design parameters on system performance. In this research work, significant parameters are selected to study their impact on the system performance, including split ratio—x, pressure ratio—π, MC inlet temperature—T_6, TB inlet temperature—T_2, and MC inlet pressure—P_6. The constraints are presented in Table 2. For the MW supercritical recompression Brayton cycle system, the split ratio, the pressure ratio, the MC inlet temperature, the TB inlet temperature, and the MC inlet pressure are important factors determining the cycle process.

For the compressor, the inlet temperature and pressure are two main factors directly affecting its work. The compressor pressure ratio also has a significant influence on the system cycle. When the pressure ratio is too high, the power consumption of the compressor will increase, and the cycle efficiency will decrease. When the pressure ratio is too small, the heat absorption of the working medium will be negligible, and the output work of the turbine will be further affected. Considering that the critical pressure of the mixed working medium is about 7.4 MPa, the data point near the critical point is selected. Therefore, the inlet pressure of the compressor is set as 7.4–8.4 MPa, and the outlet pressure of the compressor is required to be 20–30 MPa, so the pressure ratio is selected as 2.5–3.5. The inlet temperature of the turbine is related to the output work of the turbine and has a great influence on the system. In recent years, with material technology development, the turbine inlet temperature can be raised to 1423 K [32], so the turbine inlet temperature is selected as 1000–1200 K. According to relevant references, the split ratio is generally 0.25–0.35 [33].

3.5. Calculation Process of Optimization

To build a high-efficiency and economical energy system, we must comprehensively consider the balance between efficiency (energy efficiency and exergy efficiency) and total cost rate. The objective of the present work is to maximize the efficiency (η_{th} and η_{ex}) and minimize $\dot{C}_{total}$, A_{total}, and *LCOE*. The genetic algorithm (GA) [34] method optimizes the decision parameters selected to change the system performance. Figure 5 presents the optimization flowchart of the proposed system.

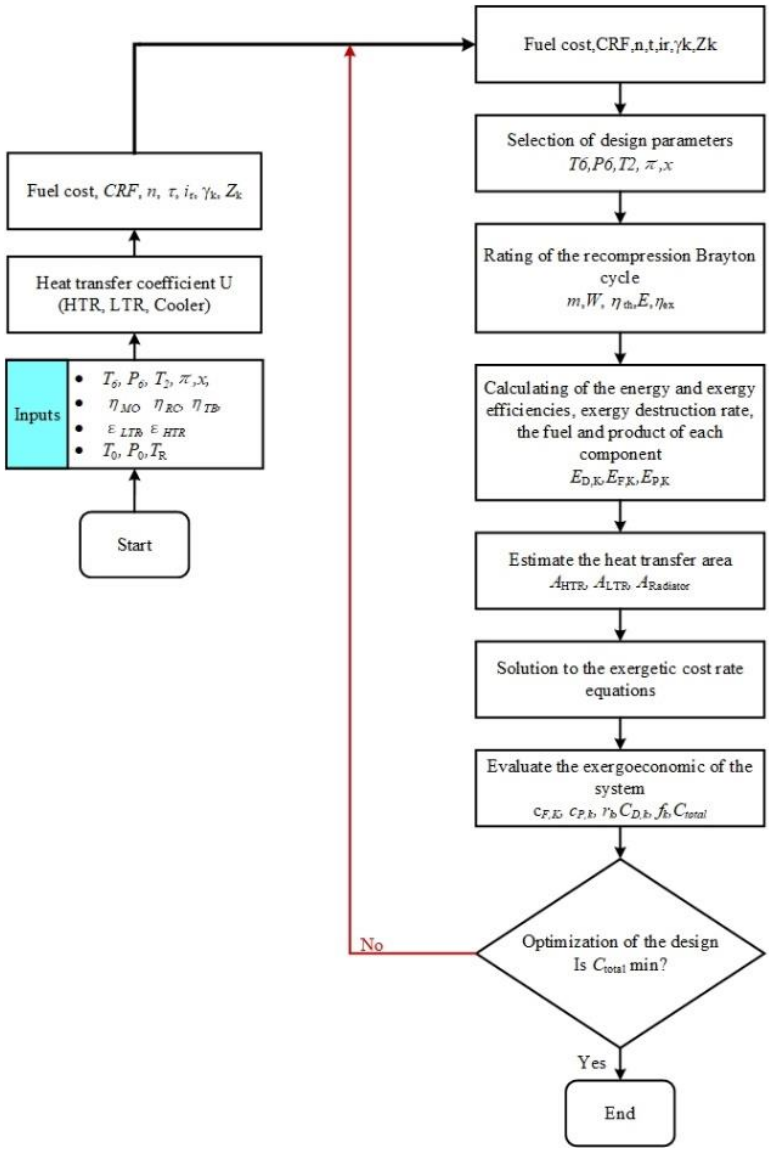

Figure 5. Optimization flowchart of the proposed S-(N_2O-He) system.

4. Results and Discussion

In this section, detailed thermodynamic and exergoeconomic analyses are presented. The thermodynamic properties of N_2O and He can be calculated using the NIST REFPROP [35] software. As the NIST REFPROP software shows, the temperature of N_2O is limited to 525 K, and to estimate the thermodynamic properties of N_2O, a thermodynamic property subroutine "PUREN2OPROP" was developed according to the previous literature report [36]. The performance of the system under different working conditions is evaluated using Excel and Python software. The basic parameters of the cycle used are listed in Table 3.

Table 3. Basic parameters selected in simulation.

Parameter Symbol	Select Value
T_0 (K)	298
P_0 (MPa)	0.101
P_6 (MPa)	7.4 [36]
m (kg/s)	1
Fuel cost ($/MWh)	7.4 [31]
η_{TB}	0.88 [13]
η_{MC}	0.85 [9]
η_{RC}	0.85 [9]
ε_{HTR}	0.86 [9]
ε_{LTR}	0.86 [9]

4.1. Energy, Exergy, and Exergoeconomic Investigation on Basic Condition

Table 4 shows the energy and exergy analysis results of the proposed cycle under typical working conditions, and the parameters are shown in Table 3. In the typical cycle, $\dot{W}_{net}$ = 0.277 MW, η_{th} = 48.14%, and η_{ex} = 64.04%. The thermodynamic characteristics, mass flow rate, and cost values of state points under the proposed cycle based on the state point numbers in Figure 2 are provided in Appendix C.

Table 4. Energy and exergy results for a basic parameters design.

Items	Value
η_{th} (%)	48.14
η_{ex} (%)	64.04
$\dot{W}_{net}$ (MW)	0.277

The exergy and exergoeconomic analyses of components are listed in Table 5. Table 5 indicates that the reactor component has a higher $\dot{Z}_j$+ $\dot{C}_{D,j}$ + $\dot{C}_{L,j}$ than other components, indicating that it should improve the reactor's exergoeconomic performance. The exergoeconomic factor value for the reactor is 56.94%, meaning that the sum of CI and OM in the reactor has an excellent ratio. The exergoeconomic factor of the turbine is 8.04%, and the value of $\dot{Z}_j$+ $\dot{C}_{D,j}$ + $\dot{C}_{L,j}$ is the second highest value. The cooler has a higher relative cost difference value than other cycle components. The cooler's exergoeconomic factor is 31.54%, which reveals that the majority cost is the exergy destruction cost in the system's total cost. Comprehensively considering overall cost values and reducing the exergy destruction of the cooler is an excellent method to change the cycle performance. The total f value of the whole cycle is 24.21%. It means that the exergy destruction reached 75.79% of the total system cost.

Table 5. Exergy and exergoeconomic results for a basic parameters design.

Components	$\dot{E}_{F,j}$ (MW)	$\dot{E}_{P,j}$ (MW)	$\dot{E}_{D,j}$ (MW)	$c_{F,j}$ ($/GJ)	$c_{P,j}$ ($/GJ)	$\dot{C}_{D,j}$ ($/h)	$\dot{Z}_j$ ($/h)	$\dot{Z}_j$+ $\dot{C}_{D,j}$+ $\dot{C}_{L,j}$ ($/h)	r_j (%)	F_j (%)
Reactor	1.977	1.901	0.076	7.782	8.172	2.130	2.817	4.947	5.01	56.94
Turbine	0.721	0.601	0.120	8.172	9.488	3.526	0.308	3.834	16.10	8.04
Main Compressor	0.225	0.186	0.038	9.488	11.908	1.305	0.069	1.374	25.51	4.99
Recompression Compressor	0.175	0.101	0.074	9.488	10.808	2.531	0.029	2.561	13.91	1.15
HTR	0.213	0.184	0.029	8.172	8.742	0.850	0.084	0.933	6.98	8.98
LTR	0.261	0.228	0.034	8.172	8.742	0.992	0.051	1.043	6.98	4.92
Cooler	0.082	0.019	0.063	8.172	28.509	1.852	0.853	2.705	248.86	31.54
System	3.653	3.220	0.434	-	-	13.186	4.212	17.397	-	24.21

4.2. Sensitivity Analysis of Main Operating Parameters

4.2.1. Influence of Split Ratio—x

Figure 6 presents the influence of x (split ratio) on η_{th}, η_{ex}, $\dot{C}_{total}$, A_{totol}, and $LCOE$. The cooling effect of the cooler and compressor power is changed by changing the split ratio with the mass flow rate change.

Figure 6a,b depict the cycle thermal and exergy efficiencies, respectively. From Figure 6a,b, under different T_6, the thermal and exergy efficiencies have the same variation trend with the increase of x, which increases slowly at first and then decreases. The η_{th} and η_{ex} are between 45.0–48.3% and 59.9–64.3%. With the increase of T_6, the η_{th} and η_{ex} decrease gradually. When x = 0.35, the efficiency (η_{th} and η_{ex}) reaches maximum with η_{th} = 48.34% and η_{ex} = 64.3%.

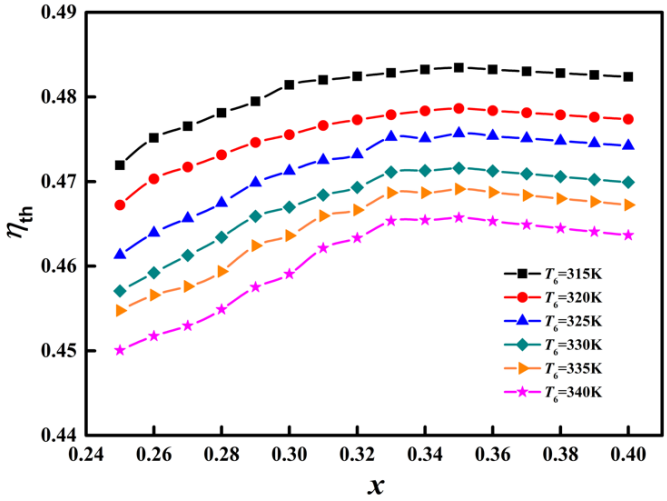

(**a**) Influence of x on η_{th}

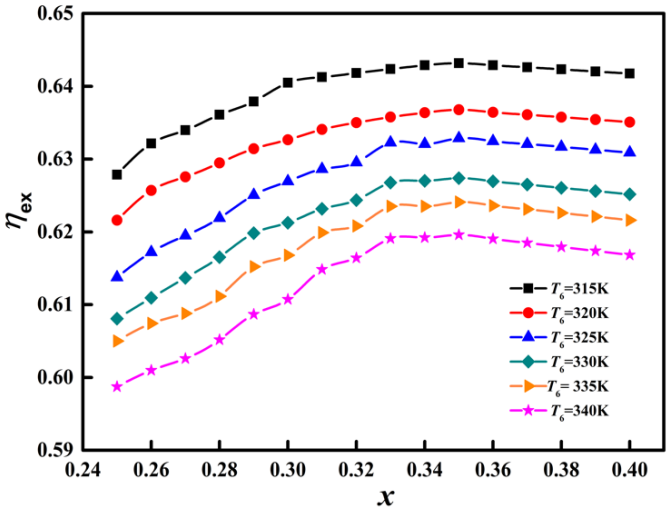

(**b**) Influence of x on η_{ex}

Figure 6. *Cont.*

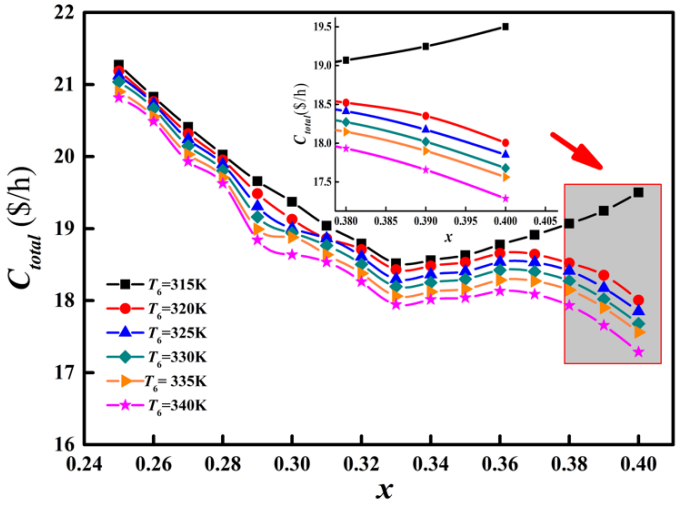

(**c**) Influence of x on $\dot{C}_{total}$

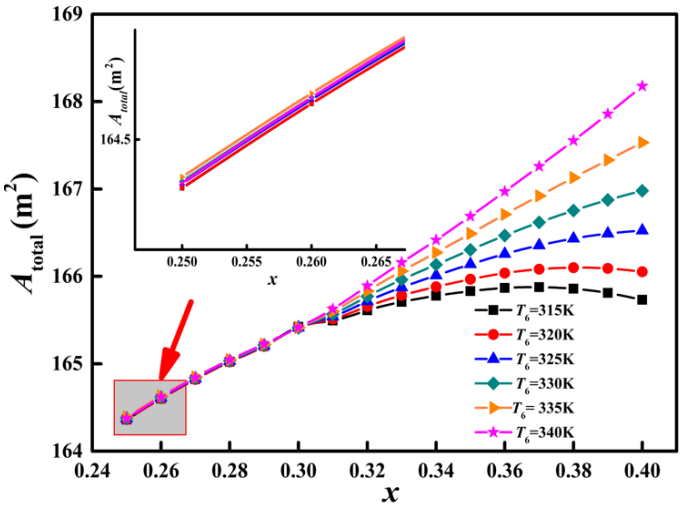

(**d**) Influence of x on A_{total}

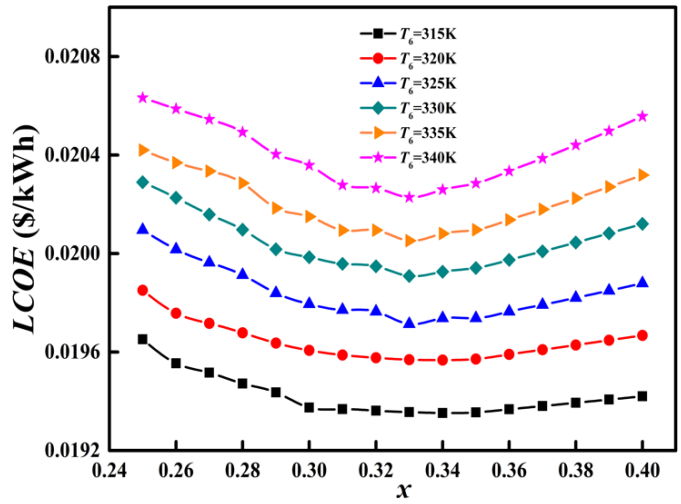

(**e**) Influence of x on *LCOE*

Figure 6. Influence of x on the proposed S-(N_2O-He) cycle.

Referring to Figure 6c, the total cost rate ($\dot{C}_{total}$) first decreased and then increased slightly; the whole variation trend decreases gently. An increase in the split ratio leads to the reduction of $\dot{C}_{D,total}$. The minimum value of $\dot{C}_{\text{total}}$ can be obtained at x = 0.33. With the increase of T_6, the $\dot{C}_{total}$ decreases, but the variation trend is not apparent. When T_6 = 315 K and x > 0.37, $\dot{C}_{total}$ increases gradually with x increases. The main reason for the change in $\dot{C}_{total}$ is that the working temperature of 315 K is near the critical point area, and the thermodynamic characteristics of the working medium at this temperature change dramatically.

The impact of the split ratio on A_{total} (the sum of the HTR heat exchange area, LTR heat exchange area, and radiator heat exchange area) is presented in Figure 6d, and the central part is the radiator area. If we change the split ratio, the total area of the heat exchange components increases with the increase of x, and the area also tends to increase with the increase of T_6. Nevertheless, as the x < 0.31, the total area has little difference. When T_6 is at the temperature of 315 K, the total heat exchanger area at a high split ratio x > 0.37 slightly decreases, which is associated with the physical properties of the working medium.

Figure 6e displays the variation trend of the *LCOE*. Under the different MC inlet temperature-T_6, with the x increasing, the *LCOE* decreased gently and at x = 0.33 achieved the lowest *LCOE*; after that split ratio, the value of *LCOE* increased slightly.

When x is small, a "pinch point" occurs at the low temperature inlet side of the HTR; when x increases, RC mass flow rate and T_5 increase, reducing the total work consumed by MC and RC. The rate of increase in net power is faster than the rate of decrease in heat absorption; then, η_{th} and η_{ex} are increased. With the increase of x, the position of the "pinch point" changes, which appears at the low temperature inlet side of LTR, and the power consumption of the RC increases alongside the increase of x. As the W_{net} decreases, η_{th} and η_{ex} decrease. With the increase of T_6 (MC inlet temperature), the compression power consumption of the whole cycle increases, resulting in the decrease of η_{th} and η_{ex}. Comprehensively considering the whole cycle, when x < 0.33, the whole W_{net} increases, and when x > 0.33, the whole W_{net} decreases. The changing trend of W_{net} results in the *LCOE* decreasing at first and increasing modestly.

4.2.2. Influence of Pressure Ratio—π

Figure 7 presents the cycle primary performance under the operating condition of x = 2.5–3.5, T_2 = 1200 K, x = 0.3, P_6 = 7.4 MPa, and T_6 = 315–340 K.

The MC inlet temperature, the compressor power consumption, and the turbine's work increase with a π increase. When the TB inlet temperature is constant at 1200 K, as the π increases, W_{net} first increases and then decreases. Moreover, the LTR outlet temperature was increased due to reduced turbine outlet temperature, increased outlet temperature in the MC, and reduced heat transfer in the recuperators. As the π increases, so does W_{net}. Therefore, η_{th} and η_{ex} first increase and then decrease with the increase of π, as presented in Figure 7a,b.

The results in Figure 7c show that an increase in π leads to an increase in $\dot{C}_{total}$ of the entire cycle, mainly due to an increase in $\dot{C}_{D,reactor}$. In addition, with the increase of π, the $\dot{C}_{D,HTR}$ decreases and $\dot{C}_{D,LTR}$ increases, and the total exergy destruction cost rate of recuperators increases due to the reduction of recuperators' heat transfer area. $\dot{Z}_j$ (CI and OM costs) of TB, MC, and RC increase by π. When π increases, the total system cost rate increases, mainly because of the rising cost of CI and OM, and $\dot{C}_{total}$. With the increase of π, the reactor and recuperators' exergy destruction cost rate increases with T_6.

According to Figure 7d, increasing π can reduce the heat transfer area of recuperators and radiators due to a decrease in heat exchange. The heat transfer area of all three components decreases, so the whole cycle heat transfer area is reduced by increasing π.

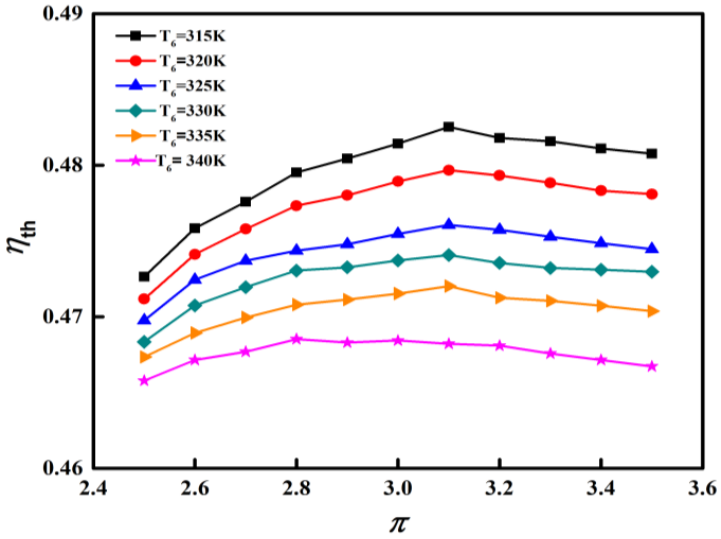

(**a**) Influence of π on η_{th}

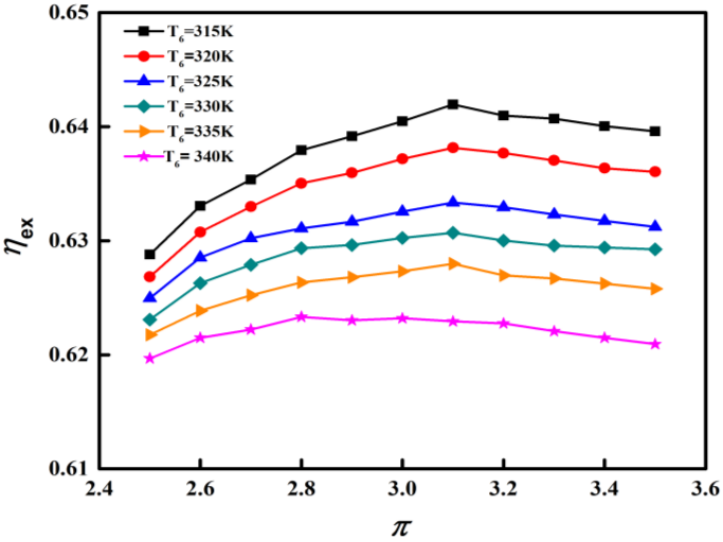

(**b**) Influence of π on η_{ex}

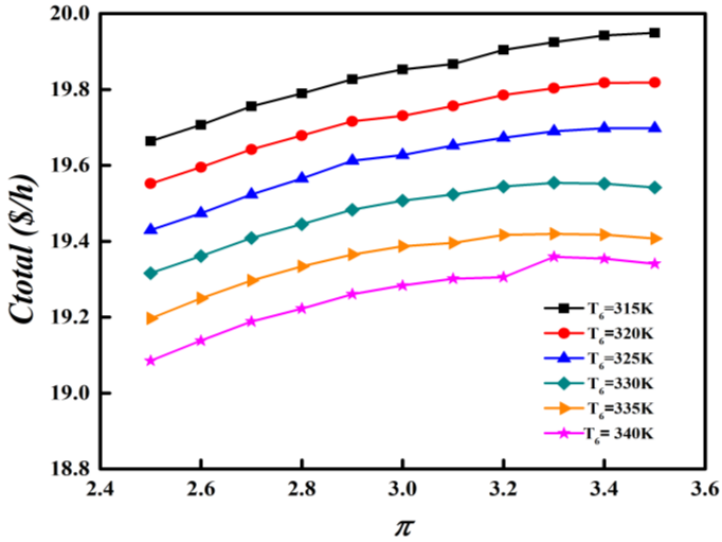

(**c**) Influence of π on $\dot{C}_{total}$

Figure 7. *Cont.*

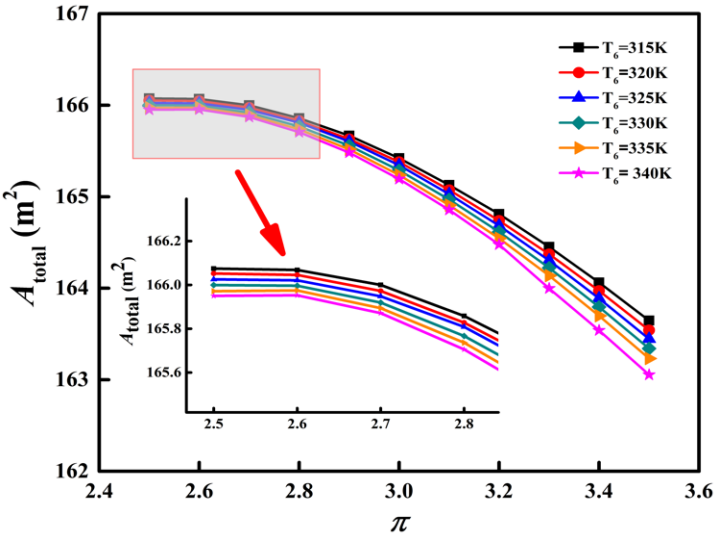

(**d**) Influence of π on A_{total}

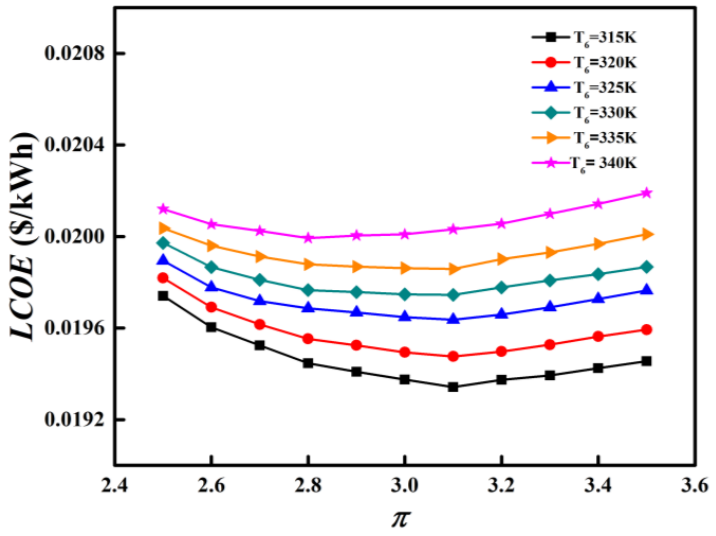

(**e**) Influence of π on *LCOE*

Figure 7. Influence of π on the proposed S-(N_2O-He) cycle.

The change of π also affects the *LCOE* of the system, as plotted in Figure 7e. The output power of TB and the whole cycle net power are increasing by increasing the π. Increasing π up to around 3.0 reduces the *LCOE* of the system, which is mainly because the system's net power value increases significantly. When π increases beyond 3.0, the net power value increase is less than the value of π below 3.0. Total investment and OM cost ($\dot{Z}_j$) of the whole cycle is increased by π increasing. However, the total cycle net power is the dominant reason for *LCOE* reduction when π is below 3.0, and *LCOE* increases in the period of π beyond 3.0, mainly due to CI and OM cost increase.

4.2.3. Influence of MC Inlet Temperature—T_6

The influence of T_6 on the cycle key performance indicators is shown in Figure 8. Figure 8a–c illustrate η_{th}, η_{ex}, and $\dot{C}_{total}$ decrease as T_6 increases. However, $\dot{C}_{total}$ is not sensitive to the change of T_6. The main reason for cyclic η_{th} and η_{ex} reduction is the difference between the maximum and minimum cyclic temperatures (Carnot principle). A higher value of T_6 leads to a higher average temperature of N_2O-He at the cooler, creating a more significant heat loss in the cooler, a higher compression work value, and a lower cycle net power. By increasing T_6, the $\dot{C}_{D,j}$ of the reactor and the cooler is reduced. At the

same time, the increase in the HTR and LTR heat transfer area will increase the $\dot{Z}_j$ value of the recuperators. Therefore, the increase of HTR and LTR cost rate is less than the decrease in the reactor and the cooler exergy destruction cost. To sum up, $\dot{C}_{total}$ of the circulating system is reduced.

A variation trend of the total heat transfer area has little influence on the increase of the MC inlet temperature, as presented in Figure 8d. Recuperators' heat transfer area is increased with the increase of T_6; nevertheless, the radiator heat transfer area decreases. The heat transfer area of the radiator decrease is greater than the increase of that in the recuperators. Therefore, A_{total} is slightly reduced.

The change of T_6 also influences the *LCOE* of the cycle, as depicted in Figure 8e. The total investment, OM costs ($\dot{Z}_j$), and whole system net power are decreased by T_6 increasing. However, the whole *LOCE* increases with a T_6 increase. The main reason for such a change is that the decrease in W_{net} is more significant than that of total investment and OM cost.

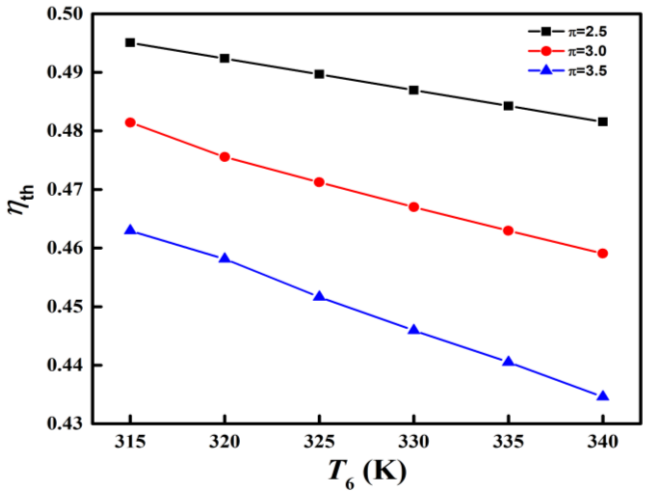

(**a**) Influence of T_6 on η_{th}

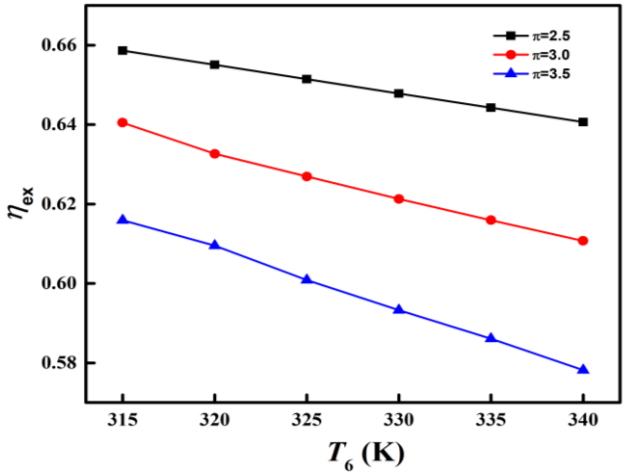

(**b**) Influence of T_6 on η_{ex}

Figure 8. *Cont.*

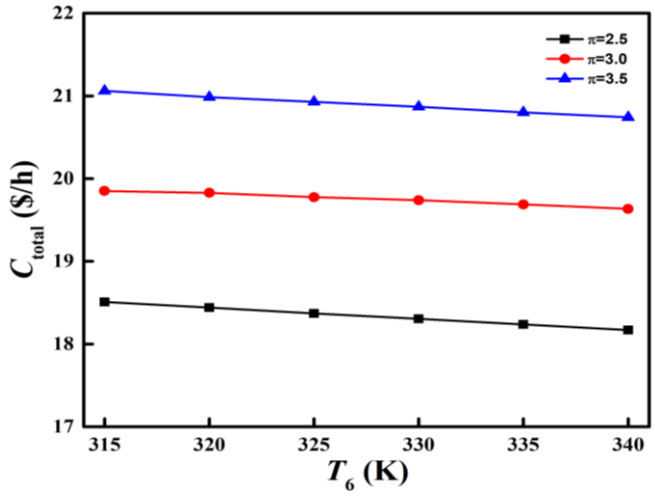

(**c**) Influence of T_6 on $\dot{C}_{total}$

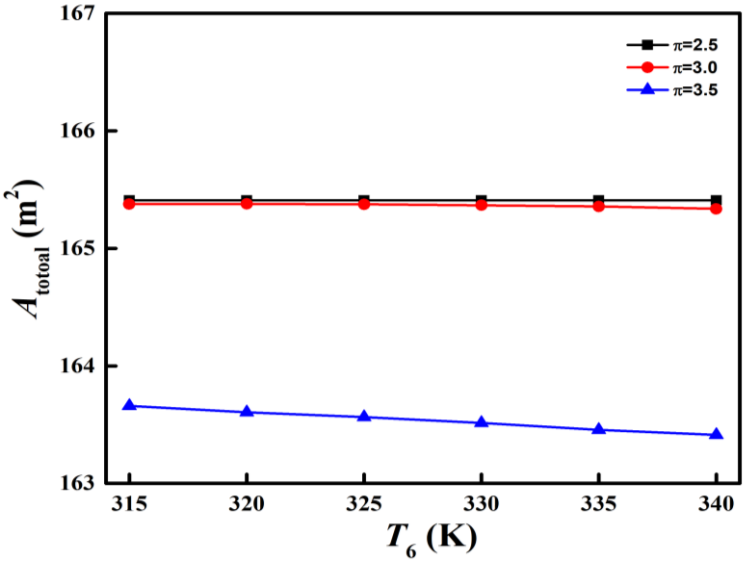

(**d**) Influence of T_6 on A_{total}

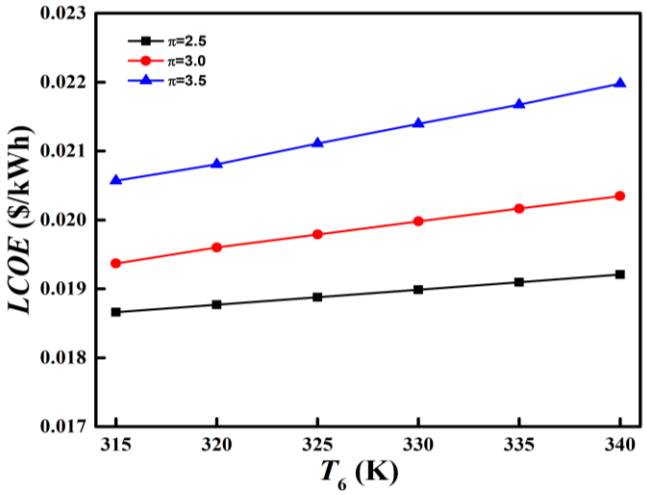

(**e**) Influence of T_6 on *LCOE*

Figure 8. Influence of T_6 on the proposed S-(N_2O-He) cycle.

4.2.4. Influence of TB Inlet Temperature—T_2

The influence of T_2 on the performance of the proposed S-(N_2O-He) cycle with x = 0.3, P_6 = 7.4 MPa, π = 3.0, and T_6 = 315–340 K is shown in Figure 9.

With the increase of T_2, the TB power output produced by the input rate of specific heat increases significantly due to the increase of TB input enthalpy. Insensitive to the effects of MC and RC work leads to an increase in W_{net} of the system. Therefore, the temperature difference between the maximum and minimum operating temperatures increases as T_2 increases, and η_{th} increases as shown in Figure 9a. The enthalpy of inflow and outflow of the reactor increases with the increases of T_2. Cycle exergy decreases with the increase of maximum operating temperature due to thermal exergy ($\dot{E}_{in}$) increase greater than net power increases, resulting in reduced exergy efficiency, as shown in Figure 9b. $\dot{C}_{total}$ is decreased, mainly caused by the decrease in $\dot{C}_{D,total}$, and the CI and OM costs of the reactor are decreased by the increase in maximum operating temperature, as displayed in Figure 9c.

Accordingly, the heat transfer of the radiator, HTR, and LTR increase with the TB inlet temperature, leading to a higher heat transfer area of these components in the system, as shown in Figure 9d. Referring to Figure 9e, *LCOE* reduces because the net power increases as T_2 increases.

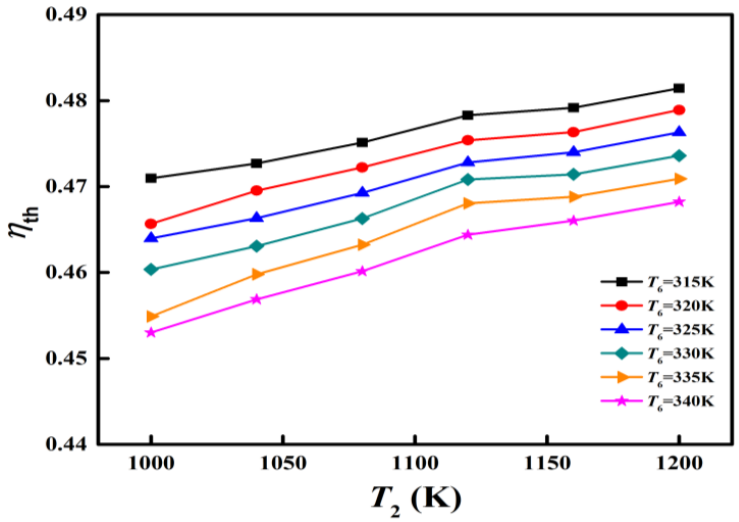

(**a**) Influence of T_2 on η_{th}

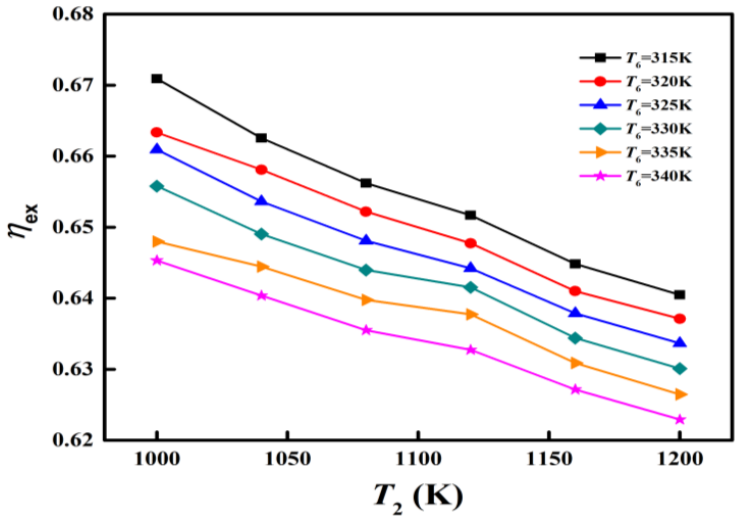

(**b**) Influence of T_2 on η_{ex}

Figure 9. *Cont.*

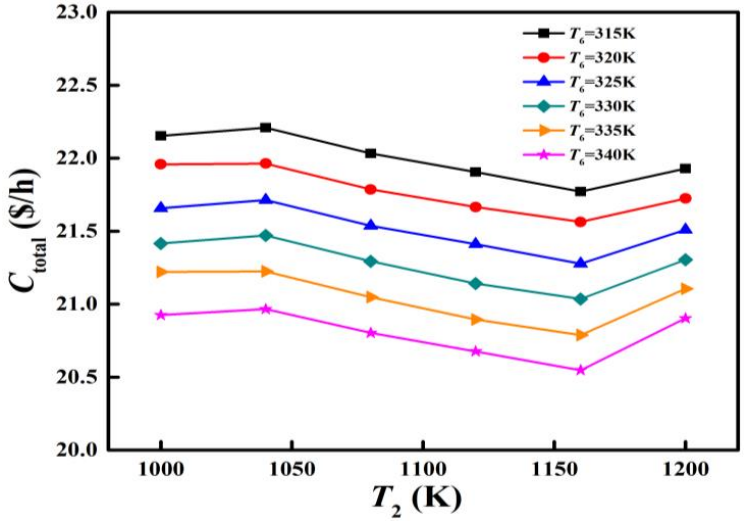

(**c**) Influence of T_2 on $\dot{C}_{total}$

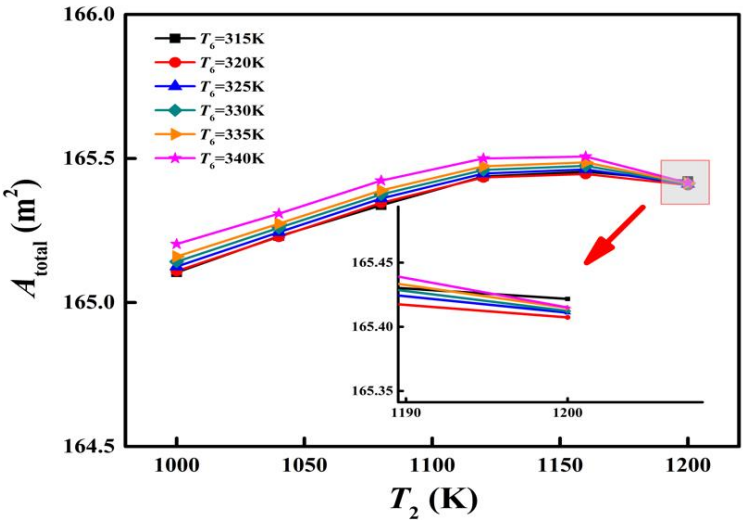

(**d**) Influence of T_2 on A_{total}

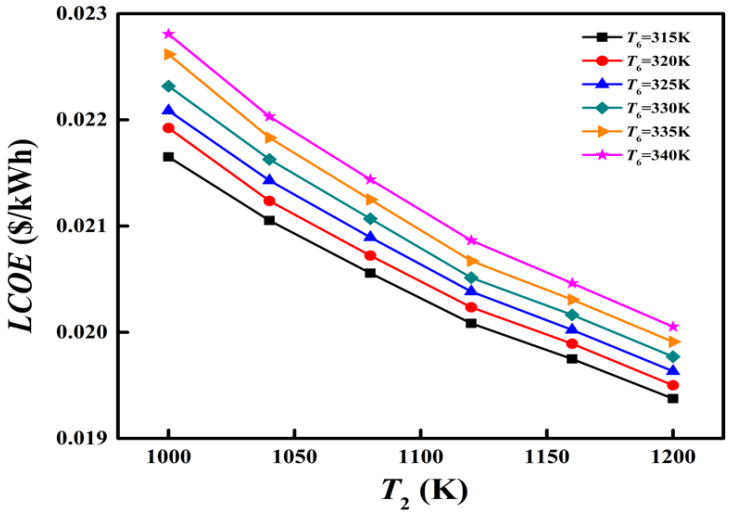

(**e**) Influence of T_2 on *LCOE*

Figure 9. Influence of T_2 on the proposed S-(N_2O-He) cycle.

4.2.5. Influence of MC Inlet Pressure—P_6

Figure 10 indicates the cycle performance variation at different P_6, T_2 = 1200 K, x = 0.3, and π = 3.0.

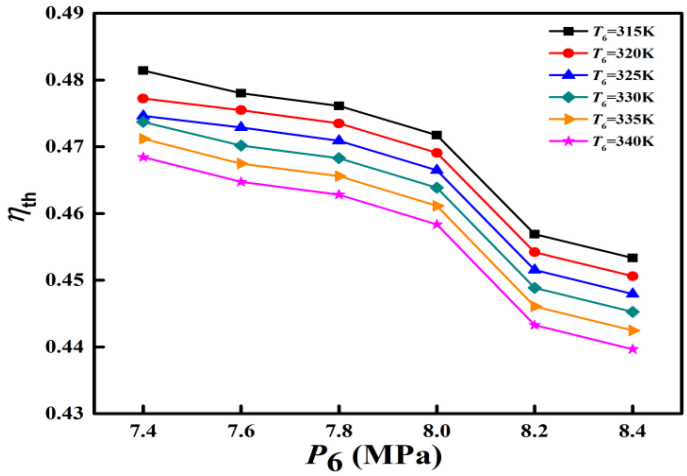

(**a**) Influence of P_6 on η_{th}

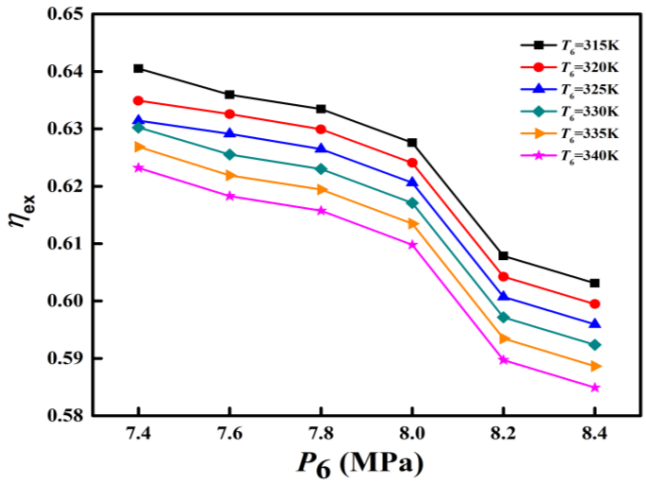

(**b**) Influence of P_6 on η_{ex}

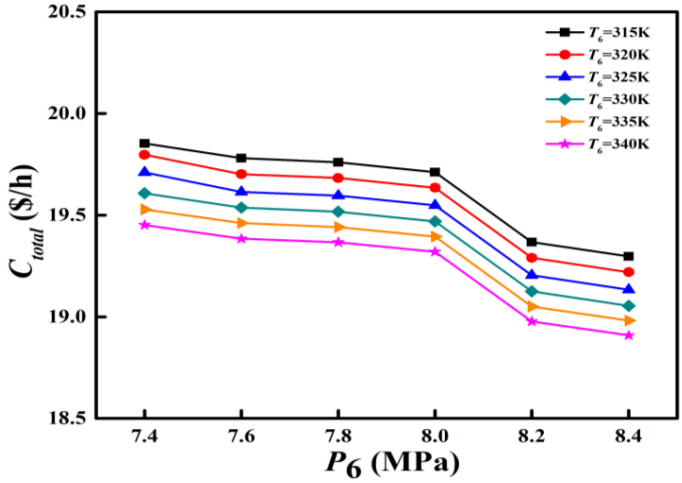

(**c**) Influence of P_6 on $\dot{C}_{total}$

Figure 10. *Cont.*

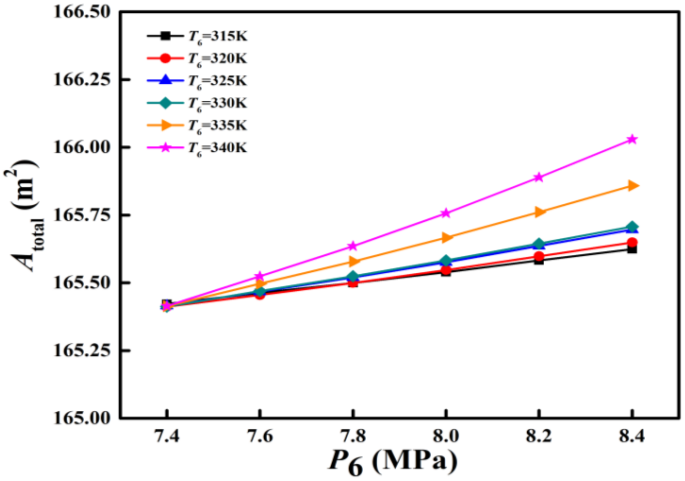

(**d**) Influence of P_6 on A_{total}

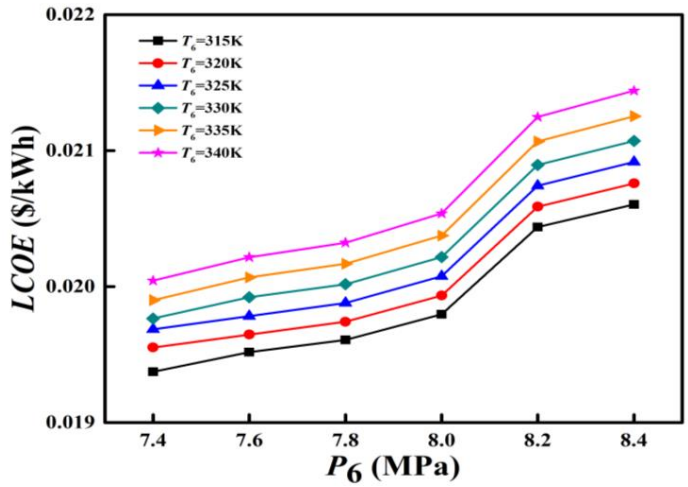

(**e**) Influence of P_6 on *LCOE*

Figure 10. Influence of P_6 on the proposed S-(N_2O-He) cycle.

η_{th} and η_{ex} decrease with increasing P_6, as presented in Figures 10a and 10b, respectively. η_{th} and η_{ex} decrease slowly and then decrease rapidly. As the working medium is worked close to the critical point area, the compression factor is small, and the consumption power of the compressor is increased, resulting in a decrease in W_{net}. The compression factor increases gradually as P_6 increases, resulting in more pressure loss, higher power consumption, and a lower net power of the cycle, thus reducing the η_{th} and η_{ex}, as shown in Figure 10a,b.

Figure 10c presents the influence of P_6 on the $\dot{C}_{total}$. As the CI and OM cost of the reactor is reduced, the total investment and OM cost is reduced, which is the highest value part of the $\dot{Z}_{total}$. $\dot{C}_{D,Reactor}$ and $\dot{C}_{D,MC}$ are also reduced. and the two components with the more significant proportion. All decreases in $\dot{Z}_{total}$ and $\dot{C}_{D,total}$ are a result of decreasing $\dot{C}_{total}$.

A_{total} is increased by the increase in P_6, as presented in Figure 10d. As P_6 increases, heat transfer in LTR and HTR increases. As a result, the heat transfer area of recuperators is also increased. The heat transfer area variation of HTR and LTR is the dominant factor causing the increase of A_{total}.

As mentioned above, W_{net} and OM costs decrease with the increase in P_6. $\dot{W}_{net}$ (net power) decreases more than $\dot{Z}_{total}$, thereby allowing a high value of *LCOE* due to an increase in MC inlet pressure.

4.3. Exergoeconomic Optimization

Based on the sensitivity analysis discussed above, η_{th} and η_{ex} improvements are always inconsistent with *LCOE*. However, in the actual thermodynamic system, efficiency (η_{th} and η_{ex}) and cycle cost are considered simultaneously. Multi-objective optimization is used to maximize thermal performance and minimize cost. For the recompression Brayton cycle, its optimization objectives are thermal efficiency $\eta_{th} = f_1(x)$, exergy efficiency $\eta_{ex} = f_2(x)$, total cost rate $\dot{C}_{total} = f_3(x)$, total area of heat transfer $A_{total} = f_4(x)$, and levelized cost of electricity $LCOE = f_5(x)$.

The response surface methodology (RSM) [21] method is utilized to make a link between the objective functions and decision parameters for optimization. The regression equation is established by experimental design and variance analysis. Finally, based on the Pareto optimality, multi-objective optimization is carried out to seek the balance between efficiency and cost.

Appropriate sample points are selected using a central composite design (CCD) [21] to approximate the response function with higher accuracy. In the CCD method, a central design point needs to be added, and the distance from the center is α. The selected decision parameters are the five test factors shown in Table 6. The Design-Expert software is used to create second-order model regression for the corresponding values of the loop.

Table 6. The partial Pareto optimal solution for η_{th} and η_{ex}.

Factor	T_6 (K)	T_2 (K)	P_6 (MPa)	π	x	η_{th} (%)	η_{ex} (%)
Optimal solution 1	337.75	1020.9	8.21	3.13	0.331	33.04	45.95
2	338.99	1001.0	8.35	3.42	0.251	32.99	45.96
3	339.99	1010.0	8.3	3.45	0.281	32.04	47.01
4	337.99	1012.0	8.1	3.49	0.332	32.05	46.95
5	338.65	1000.0	8.0	3.49	0.322	32.81	46.00
6	336.89	1020.0	8.2	3.49	0.333	33.08	45.95
7	339.99	1028.0	8.3	3.49	0.255	31.65	47.43
9	339.99	1031.0	8.4	3.49	0.325	32.88	46.98
10	338.94	1010.2	8.2	3.49	0.258	32.69	46.27
11	337.90	1020.5	8.1	3.34	0.322	32.77	46.02

Therefore, the multi-objective optimization problem of the whole loop can be defined as:

$\mathrm{Max}[f_1(x), f_2(x)]$; $\mathrm{Min}[f_3(x), f_4(x), f_5(x)]$.

The regression model functions of $\eta_{th} = f_1(x)$, $\eta_{ex} = f_2(x)$, $\dot{C}_{total} = f_3(x)$, $A_{total} = f_4(x)$, and $LCOE = f_5(x)$ are expressed as:

$$\begin{aligned} f_1(x) = \eta_{th} = \; & -342.95946 - 1.00182 \times A + 0.207314 \times B + 102.6095 \times C \\ & +18.70625 \times D + 233.2025 \times E - 0.000034 \times AB \\ & +0.0132 \times AC - 0.0512 \times AD + 0.96 \times AE \\ & -0.0115 \times BC + 0.0561 \times BD - 0.2555 \times BE \\ & -5.68 \times CD - 30.1 \times CE - 23.5 \times DE + 0.001108 \times A^2 \\ & -0.000085 \times B^2 - 4.3875 \times C^2 - 3.9575 \times D^2 \\ & +83.58333 \times E^2 \end{aligned} \tag{29}$$

$$\begin{aligned} f_2(x) = \eta_{ex} = \; & 186.98794 - 4.05654 \times A - 0.025545 \times B + 85.97158 \times C \\ & +67.343 \times D + 1105.8 \times E + 0.000136 \times AB \\ & +0.1256 \times AC - 0.0684 \times AD - 1.42 \times AE \\ & -0.01515 \times BC + 0.0595 \times BD - 0.252 \times BE \\ & -8.63 \times CD - 63.5 \times CE - 31 \times DE + 0.00522 \times A^2 \\ & -2.85417 \times 10^{-6} \times B^2 - 4.27417 \times C^2 - 8.06417 \times D^2 \\ & +406.25 \times E^2 \end{aligned} \tag{30}$$

$$\begin{aligned} f_3(x) = \dot{C}_{total} = \; & 458.17302 - 1.60636 \times A - 0.004646 \times B - 40.88086 \times C \\ & +18.39035 \times D - 161.8025 \times E - 0.000275 \times AB \\ & +0.14 \times AC + 0.0664 \times AD + 0.792 \times AE \\ & -0.001725 \times BC - 0.01184 \times BD + 0.165 \times BE \\ & -1.974 \times CD - 34.5 \times CE - 5 \times DE + 0.00052 \times A^2 \\ & +0.00004 \times B^2 + 0.770917 \times C^2 - 1.62475 \times D^2 \\ & -15.94167 \times E^2 \end{aligned} \tag{31}$$

$$\begin{aligned} f_4(x) = A_{total} = \; & 120.48618 + 0.278564 \times A + 0.009831 \times B - 2.801 \times C \\ & +6.75212 \times D - 46.054 \times E + 0.000048 \times AB \\ & +0.0136 \times AC - 0.01036 \times AD - 0.028 \times AE \\ & +0.001272 \times BC + 0.00016 \times BD + 0.001 \times BE \\ & -0.1989 \times CD + 5.3 \times CE + 38 \times DE - 0.000598 \times A^2 \\ & -0.000016 \times B^2 - 0.24075 \times C^2 - 2.49298 \times D^2 \\ & -151.70167 \times E^2 \end{aligned} \tag{32}$$

$$\begin{aligned} f_5(x) = LCOE \; & = 0.1 * (-33.32761 + 0.126413 \times A + 0.006422 \times B \\ & +1.82567 \times C + 0.731167 \times D + 7.04317 \times E \\ & +2.0 \times 10^{-9} \times AB + 0.000043 \times AC + 0.000034 \times AD \\ & -0.00056 \times AE + 4.6 \times 10^{-6} \times BC - 0.000053 \times BD \\ & +0.000201 \times BE + 0.000148 \times CD + 0.005 \times CE \\ & +0.031 \times DE - 0.000193 \times A^2 - 2.89721 \times 10^{-6} \times B^2 \\ & -0.117088 \times C^2 - 0.116345 \times D^2 - 12.02983 \times E^2) \end{aligned} \tag{33}$$

where A—MC inlet temperature T_6, B—TB inlet temperature T_2, C—MC inlet pressure P_6, D—compressor pressure ratio π, and E—split ratio x.

4.3.1. Dual Objective Optimization of η_{th} and η_{ex}

Firstly, the system's thermodynamic performance is considered by using the dual-objective optimization method. Taking the cycle's η_{th}—$f_1(x)$ and η_{ex}—$f_2(x)$ as the response targets, the functions are defined in Equations (29) and (30).

In the process of dual-objective optimization, the initial population size is 1000, the crossover factor is 0.7, and the variation factor is 0.3. The whole Pareto front of η_{th} and η_{ex} has 300 data in Figure 11 and partial data are shown in Table 6. After considering the η_{th} and η_{ex}, we select the final optimization result.

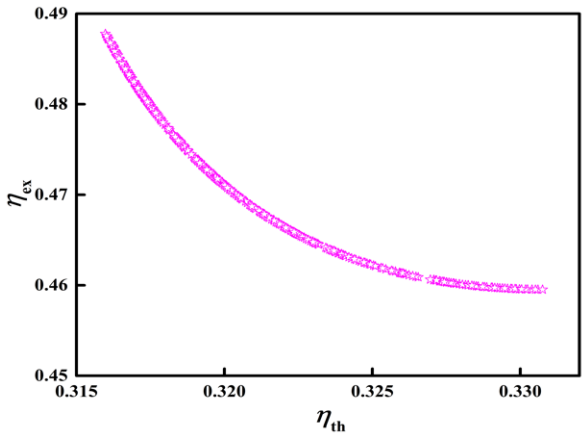

Figure 11. Pareto optimal solution for η_{th} and η_{ex}.

4.3.2. Three Objectives Optimization of η_{th} and η_{ex}, and $\dot{C}_{total}$

Figure 12 and Table 7 present the three objectives optimization results of η_{th}—$f_1(x)$, η_{ex}—$f_2(x)$, and $\dot{C}_{total}$—$f_3(x)$. The optimized functions are Equations (29), (30), and (31).

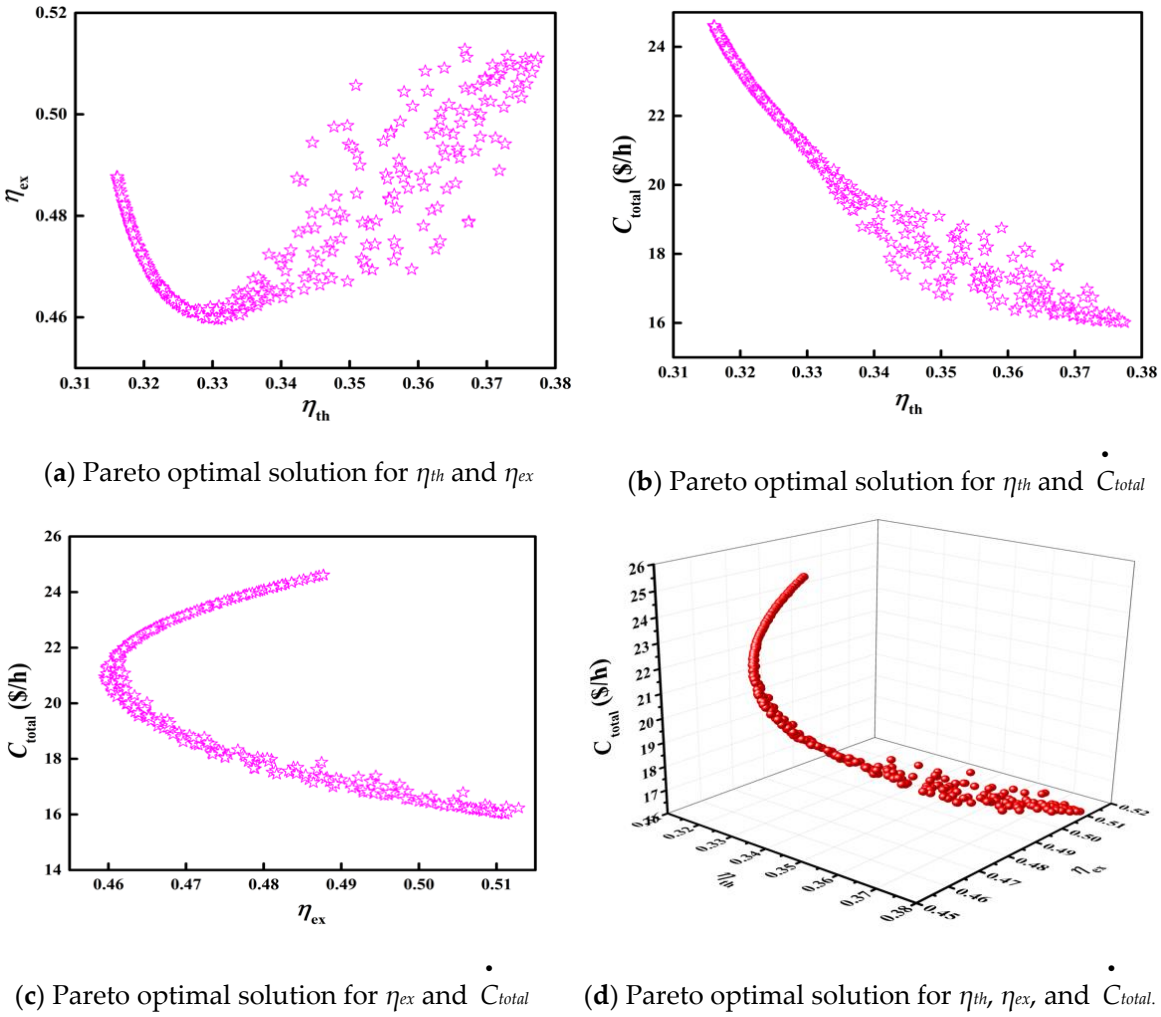

(**a**) Pareto optimal solution for η_{th} and η_{ex}

(**b**) Pareto optimal solution for η_{th} and $\dot{C}_{total}$

(**c**) Pareto optimal solution for η_{ex} and $\dot{C}_{total}$

(**d**) Pareto optimal solution for η_{th}, η_{ex}, and $\dot{C}_{total.}$

Figure 12. Three objectives Pareto optimal solution for η_{th}, η_{ex}, and $\dot{C}_{total}$.

Table 7. Pareto optimal solution for η_{th}, η_{ex}, and $\dot{C}_{total}$.

Factor	T_6 (K)	T_2 (K)	P_6 (MPa)	π	x	η_{th} (%)	η_{ex} (%)	$\dot{C}_{total}$ ($/h)
Optimal solution 1	315.0	1117.71	8.3	3.4	0.349	37.74	51.11	16.01
2	317.5	1086.14	8.4	3.5	0.347	36.97	50.27	16.36
3	315.0	1112.47	8.4	3.5	0.345	37.65	51.09	16.01
4	315.1	1095.63	8.3	3.4	0.349	37.47	51.23	16.06
5	315.1	1065.91	8.3	3.5	0.349	36.70	50.95	16.17
6	315.6	1091.51	8.2	3.4	0.349	37.31	50.98	16.13
7	319.1	1065.93	8.3	3.3	0.346	36.49	49.89	16.69
8	318.3	1077.11	8.2	3.3	0.325	36.85	50.21	16.51
9	322.5	1066.45	8.3	3.5	0.348	36.24	48.96	17.10
10	321.8	1016.96	8.3	3.4	0.348	34.79	48.84	17.45

In the three objectives optimization, the initial population size is 1000, the crossover factor is 0.7, and the variation factor is 0.3. Figure 12a–c show the Pareto optimal boundary, which η_{th} and η_{ex}, η_{th} and $\dot{C}_{total}$, and η_{ex} and $\dot{C}_{total}$ are the optimization objectives, respectively. Figure 12d considers the Pareto solution of η_{th}, η_{ex}, and $\dot{C}_{total}$.

4.3.3. Three Objectives Optimization of η_{th}, η_{ex}, and A_{total}

The three objectives optimization between η_{th}–$f_1(x)$, η_{ex}–$f_2(x)$, and A_{total}–$f_4(x)$ are shown in Figure 13 and Table 8. The optimized functions are Equations (29), (30), and (32).

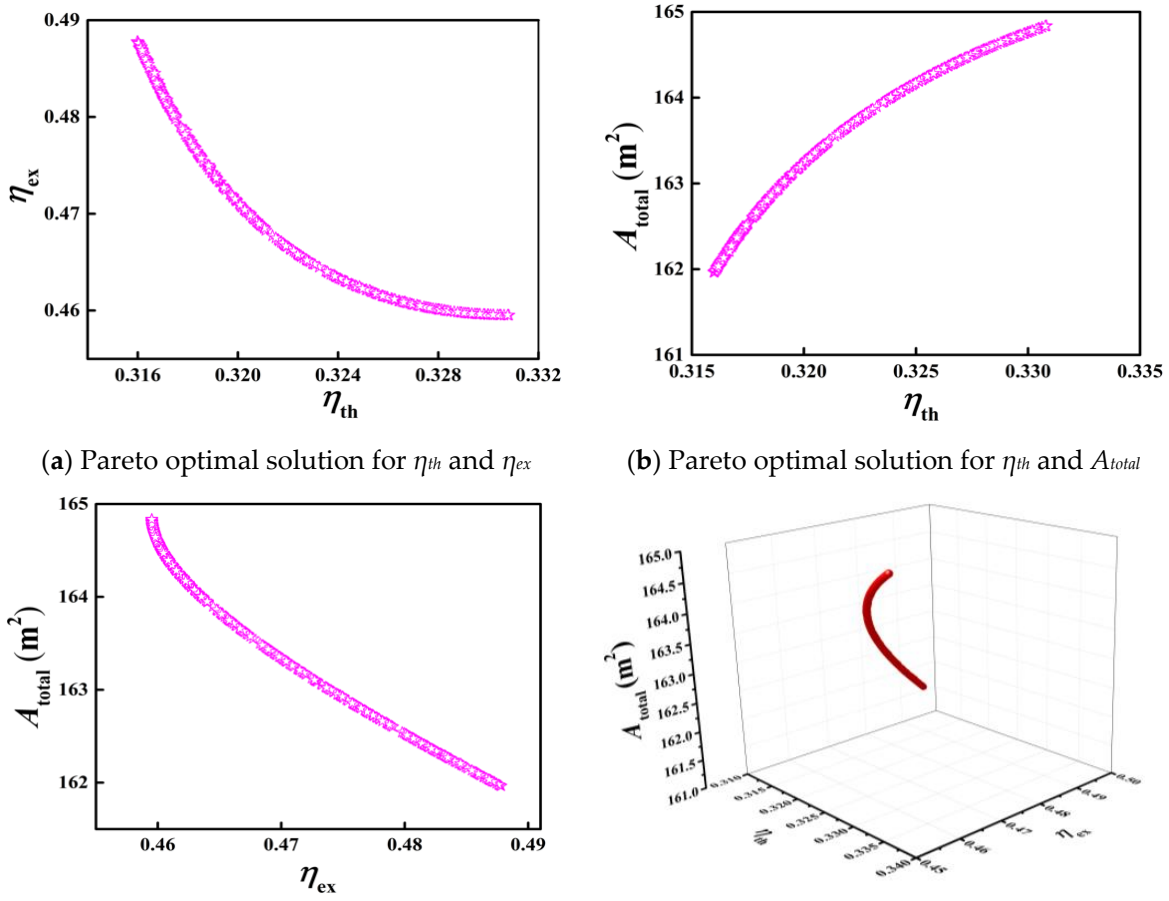

(**a**) Pareto optimal solution for η_{th} and η_{ex}

(**b**) Pareto optimal solution for η_{th} and A_{total}

(**c**) Pareto optimal solution for η_{ex} and A_{total}

(**d**) Pareto optimal solution for η_{th}, η_{ex}, and A_{total}

Figure 13. Three objectives Pareto optimal solution for η_{th}, η_{ex}, and A_{total}.

Table 8. Pareto optimal solution for η_{th}, η_{ex}, and A_{total}.

Factor	T_6 (K)	T_2 (K)	P_6 (MPa)	π	x	η_{th} (%)	η_{ex} (%)	A_{total} (m^2)
Optimal solution 1	337.0	1004.2	8.3	3.35	0.333	33.08	45.95	164.83
2	335.2	1020.3	8.4	3.45	0.302	32.39	46.34	164.01
3	337.5	1010.5	8.2	3.46	0.323	32.84	46.00	164.60
4	338.9	1078.6	8.2	3.42	0.332	33.04	45.95	164.80
5	339.1	1025.3	8.4	3.48	0.331	33.02	45.95	164.78

In the three objectives optimization, the initial population size is 1000, the crossover factor is 0.7, and the variation factor is 0.3. Figure 13a–c show the Pareto optimal boundary with η_{th} and η_{ex}, η_{th} and A_{total}, and η_{ex} and A_{total} as the optimization objectives. Figure 13d considers the Pareto solution of the three objectives of η_{th}, η_{ex}, and A_{total}.

4.3.4. Three Objectives Optimization of η_{th}, η_{ex}, and *LCOE*

The result of three objectives, optimization of η_{th}–$f_1(x)$, η_{ex}–$f_2(x)$, and *LCOE*–$f_5(x)$, are shown in Table 9. Figure 14 depicts the Pareto frontier for the three objectives optimization. The optimized functions are Equations (29), (30), and (33).

Table 9. Pareto optimal solution for η_{th}, η_{ex}, and *LCOE*.

Factor	T_6 (K)	T_2 (K)	P_6 (MPa)	π	x	η_{th} (%)	η_{ex} (%)	*LCOE* ($/kWh)
Optimal solution 1	315.04	1000.13	7.4	2.58	0.258	48.77	67.16	0.01732
2	315.01	1000.16	7.4	2.55	0.252	49.08	67.41	0.01697
3	315.03	1000.32	7.4	2.56	0.255	49.24	67.12	0.01792
4	317.02	1002.89	7.4	2.52	0.263	49.30	67.56	0.01680
5	318.03	1010.16	7.4	2.56	0.265	48.92	67.28	0.01719
6	315.12	1000.59	8.4	2.51	0.251	53.51	72.92	0.01640
7	315.01	1000.89	7.4	2.51	0.268	49.45	67.68	0.01654
8	316	1000.46	7.4	2.52	0.255	49.36	67.62	0.01662

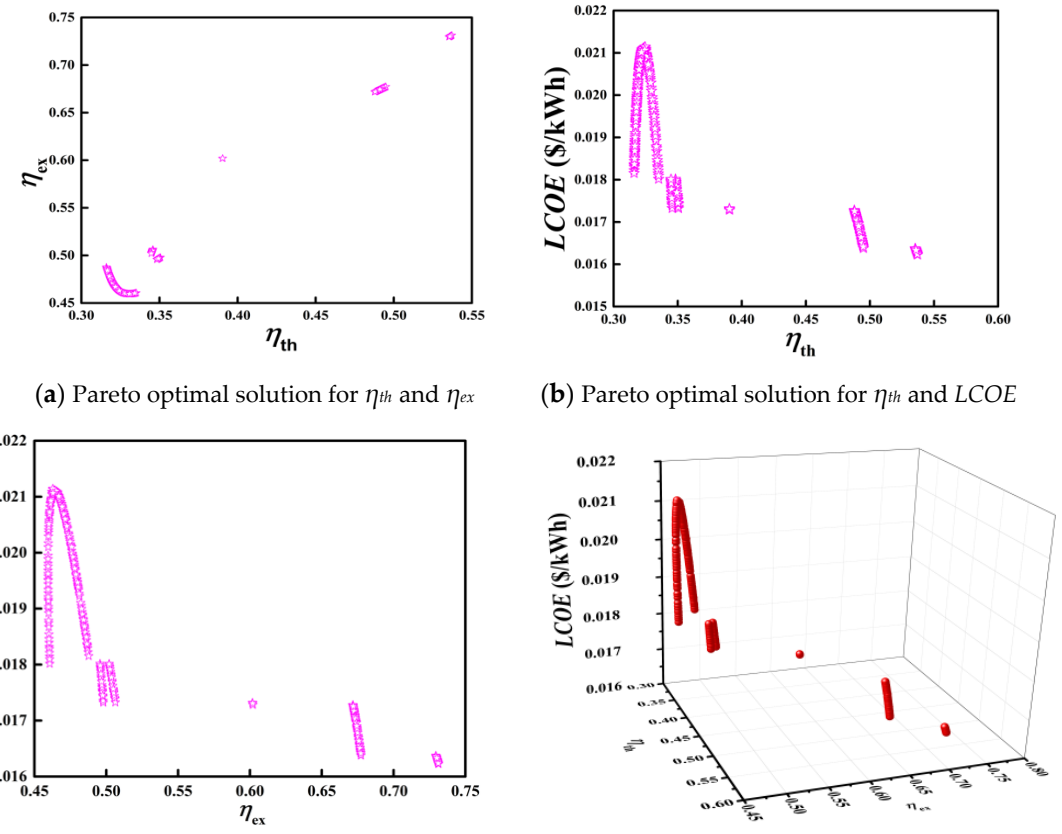

(**a**) Pareto optimal solution for η_{th} and η_{ex}

(**b**) Pareto optimal solution for η_{th} and *LCOE*

(**c**) Pareto optimal solution for η_{ex} and *LCOE*

(**d**) Pareto optimal solution for η_{th}, η_{ex}, and *LCOE*

Figure 14. Three objectives Pareto optimal solution for η_{th}, η_{ex}, and *LCOE*.

In the three objectives optimization, the initial population size is 1000, the crossover factor is 0.7, and the variation factor is 0.3. Figure 14a–c shows the Pareto optimal boundary, with η_{th} and η_{ex}, η_{th} and *LCOE*, and η_{ex} and *LCOE* as the optimization objectives, respectively. Figure 14d considers the Pareto solution of three objectives: η_{th}, η_{ex}, and *LCOE*. In practical application, suitable operating parameters can be selected according to specific conditions and requirements.

According to this part, multi-optimization and comprehensiveness consider the optimization results, and the final vital parameters of the proposed S-(N_2O-He) cycle are selected and detailed in Table 10.

Table 10. Final results of the key optimization parameters.

Factor	T_6 (K)	T_2 (K)	P_6 (MPa)	π	x	η_{th} (%)	η_{ex} (%)	$\dot{C}_{total}$ ($/h)	A_{total} (m^2)	*LCOE* ($/kWh)
Optimal solution	316.5	1010	7.4	2.58	0.26	49.14	67.29	19.37	165.55	0.0196

Table 11 shows the optimization operation parameters and performance metrics after the optimization process, while other conditions are under the same primary operating conditions.

Table 11. Key operating parameters after cycle optimization design.

Parameter	Value in Basic Case	Value in Optimization Case	Change from the Base Case (%)
T_6 (K)	315	316.5	0.48
T_2 (K)	1200	1010	−15.83
P_6 (MPa)	7.4	7.4	0
π	3.0	2.58	−14.00
x	0.3	0.26	−13.33
$\dot{W}$ (MW)	0.227	0.364	+60.35
η_{th} (%)	48.14	49.14	+2.08
η_{ex} (%)	64.04	67.29	+5.07
$\dot{C}_{total}$ ($/h)	22.52	19.37	−13.99
A_{total} (m^2)	165.57	165.55	−0.01
LCOE ($/kWh)	0.02066	0.0196	−5.13

5. Conclusions

A supercritical recompression Brayton cycle with 85% N_2O–15% He as the working medium is used for detailed thermodynamic analysis, exergoeconomic analysis, and parametric optimization. The sensitivity analysis and study of cycle parameters are carried out to study the influence of critical thermodynamic parameters on efficiency (η_{th} and η_{ex}), $\dot{C}_{total}$, A_{total}, and *LCOE*. Then, dual-objective and multi-objective function optimization is performed out of the loop. The multi-objective is based on the Pareto frontier, selecting η_{th}, η_{ex}, $\dot{C}_{total}$, A_{total}, and *LCOE* as the objective functions. At the same time, the essential parameters studied are selected as decision variables. For this work, to evaluate the thermodynamic and exergoeconimic performance, the results can be listed as follows:

1. The exergy destruction rates in the reactor, TB, and RC are higher than the value in other components.
2. The reactor and turbine have larger values of $\dot{Z}_j + \dot{C}_{D,j} + \dot{C}_{L,j}$ than other components in the cycle, which can be effectively reduced with a split ratio increase, TB inlet temperature, and MC inlet pressure.
3. Compared with the initial basic design, η_{th} and η_{ex} improved by 2.08% and 5.07% when optimized based on the first and second laws of thermodynamics.
4. When optimized based on the exergy economics, the sum of the system $\dot{C}_{total}$ is reduced by 13.99%.
5. When the cycle operates on the optimized conditions, the net power increases by 60.35%. Based on the critical parametric analysis, the total heat transfer area and *LCOE* decrease by 0.01% and 5.13%.

Considering the particularity of the space system, it is necessary to focus on the mass characteristics of the nuclear power system and use the radiator model, exergoeconomic model, and levelized cost of electricity model to make a quantitative evaluation of its volume characteristics, economic cost characteristics, and power generation cost characteristics. The parametric sensitivity analysis concluded that there is always a contradiction between the thermal and economic performance of the system. Therefore, a multi-objective

optimization method based on the Pareto frontier is used to determine the optimal operating condition and design parameters. Minimizing the total cost and maximizing the overall thermal and exergy efficiency reduces the total product unit cost and *LCOE* price. The proposed 85% N_2O–15% He recompression Brayton cycle could produce net power of 0.364 MW with a thermal efficiency of 49.14% at a *LOCE* price of USD 0.0196/kWh. The thermal efficiency is increased by 15.66%, and the *LCOE* price is reduced by 52.3% compared with the S-CO_2 recompression Brayton cycle under the same operating conditions. Accordingly, the performance of the proposed cycle is promising and can offer a potential working fluid selection for the space nuclear power system in the near future.

Author Contributions: Conceptualization, X.M. and H.Z.; formal analysis, X.M. and Y.X.; investigation, X.M.; methodology, X.M., Q.W. and W.S.; software, X.M.; writing—original draft, X.M.; funding acquisition, H.Z. and Y.X.; supervision, H.Z. and Y.X.; data curation, Q.W. and W.S.; resources, Q.W. All authors have read and agreed to the published version of the manuscript.

Funding: This research was funded by National Key R&D Program of China, Grant number 2020YFB1901800.

Data Availability Statement: Not applicable.

Conflicts of Interest: The authors declare no conflict of interest.

Appendix A. Energy and Exergy Balance Equations of the System Components

For the energy and exergy analysis, the calculation equations for each system component are listed in Table A1.

Table A1. Energy balance and exergy balance calculation equations of circulating components.

Components	Energy Conservation Equation	Exergy Destruction ($\dot{E}_F - \dot{E}_P$)
Reactor	$\dot{Q}_R = \dot{m}_1(h_2 - h_1)$	$\dot{E}_{D,R} = (\dot{E}_1 + \dot{E}_{Q_R}) - \dot{E}_2$
Turbine	$\dot{W}_T = \dot{m}_2(h_3 - h_2)$ $\eta_T = \frac{h_2 - h_3}{h_2 - h_{3s}}$	$\dot{E}_{D,T} = (\dot{E}_2 - \dot{E}_3) - \dot{W}_T$
Main Compressor	$\dot{W}_{MC} = \dot{m}_7(h_7 - h_6)$ $\eta_{MC} = \frac{h_{7s} - h_6}{h_7 - h_6}$	$\dot{E}_{D,MC} = \dot{W}_{MC} - (\dot{E}_7 - \dot{E}_6)$
Recompression Compressor	$\dot{W}_{RC} = \dot{m}_{5b}(h_8 - h_5)$ $\dot{W}_{RC} = \dot{m}_{5b}(h_8 - h_5)$	$\dot{E}_{D,RC} = \dot{W}_{RC} - (\dot{E}_{8b} - \dot{E}_{5b})$
HTR	$\varepsilon_{HTR} = \frac{T_3 - T_4}{T_3 - T_8}$ $h_3 - h_4 = h_1 - h_8$	$\dot{E}_{D,HTR} = (\dot{E}_3 - \dot{E}_4) - (\dot{E}_1 - \dot{E}_8)$
LTR	$\varepsilon_{LTR} = \frac{T_4 - T_5}{T_4 - T_7}$ $\dot{m}_4(h_{8a} - h_7) = \dot{m}_7(h_4 - h_5)$	$\dot{E}_{D,LTR} = (\dot{E}_4 - \dot{E}_5) - (\dot{E}_{8a} - \dot{E}_7)$
Cooler	$\dot{m}_{5a}(h_5 - h_6) = \dot{m}_9(h_{10} - h_9)$	$\dot{E}_{D,Cooler} = (\dot{E}_{5a} - \dot{E}_6) - (\dot{E}_{10} - \dot{E}_9)$

Appendix B. Investment Cost of the System Components

For the exergoeconomic analysis, several calculation equations are used to estimate the investment costs of each system's main components. The investment cost is expressed as a function of the appropriate thermodynamic variables. The investment cost equations for each component of the proposed system are given in Table A2.

Table A2. CI cost equations and economic value of each component [37,38].

Components	CI Cost Equation ($Z_{original}$)
Reactor	$Z_R = c_R * \dot{Q}_R,\ c_R = 283\ \$/kW$
Turbine	$Z_{TB} = 479.34 * \dot{m}_2 * [1/(0.93 - \eta_T)] * ln(\pi) * [1 + exp(0.036 * T_2 - 54.4)]$
Main Compressor	$Z_{MC} = 71.1 * \dot{m}_6 * [1/(0.92 - \eta_{MC})] * \pi * ln(\pi)$
Recompression Compressor	$Z_{RC} = 71.1 * \dot{m}_{5b} * [1/(0.92 - \eta_{MC})] * \pi * ln(\pi)$
HTR	$Z_{HTR} = 2681 * A_{HTR}^{0.59}$
LTR	$Z_{LTR} = 2681 * A_{LTR}^{0.59}$
Cooler	$Z_{Cooler} = 2143 * A_{Cooler}^{0.514}$
Factor	**Value**
Number of system operation years (n)	20
Annual system working hours (τ)	8000
Interest rate of system (i_r)	12%
Maintenance factor (i_k)	0.06
Capital recovery factor (CRF)	$CRF = \frac{i_r * (1+i_r)^n}{(1+i_r)^n - 1}$

The cost analysis for the circulatory system's different components of the cycle and auxiliary equations required for the exergy analysis are all presented in Table A3. As shown in Table A4, several vital indicators are used to identify economic behavior.

Table A3. Exergy balance for system different components and required auxiliary equations.

Components	Exergy Balance Equation	Auxiliary Equation
Reactor	$\dot{C}_2 = \dot{C}_{Fuel} + \dot{C}_1 + \dot{Z}_R$	non
Turbine	$\dot{C}_3 + \dot{C}_{TB} = \dot{C}_2 + \dot{Z}_{TB}$	$\frac{\dot{C}_3}{\dot{E}_3} = \frac{\dot{C}_2}{\dot{E}_2}$, or $c_2 = c_3$
Main Compressor	$\dot{C}_7 = \dot{C}_{MC} + \dot{C}_6 + \dot{Z}_{MC}$	$\frac{\dot{C}_{W_{MC}}}{\dot{W}_{MC}} = \frac{\dot{C}_{W_{TB}}}{\dot{W}_{TB}}$, or $c_{MC} = c_{TB}$
Recompression Compressor	$\dot{C}_{8b} = \dot{C}_{RC} + \dot{C}_{5b} + \dot{Z}_{RC}$	$\frac{\dot{C}_{W_{RC}}}{\dot{W}_{RC}} = \frac{\dot{C}_{W_{TB}}}{\dot{W}_{TB}}$, or $c_{RC} = c_{TB}\ \dot{C}_{5b} = x\dot{C}_5$
HTR	$\dot{C}_1 + \dot{C}_4 = \dot{C}_8 + \dot{C}_3 + \dot{Z}_{HTR}$	$\frac{\dot{C}_3}{\dot{E}_3} = \frac{\dot{C}_4}{\dot{E}_4}$, or $c_3 = c_4\ \dot{C}_8 = \dot{C}_{8a} + \dot{C}_{8b}$
LTR	$\dot{C}_5 + \dot{C}_{8a} = \dot{C}_7 + \dot{C}_4 + \dot{Z}_{LTR}$	$\frac{\dot{C}_4}{\dot{E}_4} = \frac{\dot{C}_5}{\dot{E}_5}$, or $c_4 = c_5$
Cooler	$\dot{C}_6 + \dot{C}_{10} = \dot{C}_9 + \dot{C}_{5a} + \dot{Z}_{Cooler}$	$\frac{\dot{C}_6}{\dot{E}_6} = \frac{\dot{C}_{5a}}{\dot{E}_{5a}}$, or $c_6 = c_{5a}\ \dot{C}_9 = 0$, $\dot{C}_{5a} = (1-x)\dot{C}_5$

Table A4. Exergoeconomic evaluation parameters [26,27].

Average exergy cost per unit of fuel	$c_{F,j} = \dot{C}_{F,j} / \dot{E}_{F,j}$
Average exergy cost per unit of product	$c_{P,j} = \dot{C}_{P,j} / \dot{E}_{P,j}$
Relative cost difference	$r_j = (c_{P,j} - c_{F,j}) / c_{F,j}$
Exergy destruction cost rate	$\dot{C}_{D,j} = c_{F,j} \times \dot{E}_{D,j}$
Exergy economic factor	$f_j = \dot{Z}_j / (\dot{Z}_j + \dot{C}_{D,j} + \dot{C}_{L,j})$
Total cost rate	$\dot{C}_{total} = \sum_j \dot{Z}_j + \sum_j \dot{C}_{D,j}$

Appendix C. Thermodynamic Characteristics of Cycle State Point

Table A5 lists the thermodynamic characteristics, mass flow rate, and cost values of state points under the proposed cycle based on the state point numbers in Figure 2.

Table A5. Thermodynamic characteristics at different cycle state point.

State Point	T (K)	P (MPa)	$\dot{m}$ (kg/s)	h (kJ/kg)	s (kJ/kgK)	$\dot{E}$ (MW)	Costs	
							$\dot{C}$ ($/h)	c ($/GJ)
1	955.7	22.2	1	1790.9	6.13	1.198	37.848	8.772
2	1200	22.2	1	2366.2	6.61	1.631	47.988	8.173
3	943.2	7.4	1	1765.4	6.11	0.959	28.214	8.173
4	860.9	7.4	1	1544.1	5.89	1.023	30.107	8.173
5	528.1	7.4	1	985.2	5.08	0.706	20.785	8.173
6	315	7.4	0.7	568.2	4.07	0.413	8.499	5.720
7	473.9	22.2	0.7	889.1	4.89	0.468	16.419	9.745
8	847.5	22.2	1	1569.6	5.92	1.041	39.44	10.518
9	298	0.1	1.5	629.4	6.26	0	0	0
10	437.1	0.1	1.5	824	6.85	0.025	2.572	28.509
$\dot{W}_{TB}$	-	-	-	-	-	-	20.521	9.488
$\dot{W}_{MC}$	-	-	-	-	-	-	7.673	9.488
$\dot{W}_{RC}$	-	-	-	-	-	-	5.989	9.488

References

1. Zhang, H.; Yin, D.; Chai, X.; Kong, B.; Liu, X. Thermoelectric conversion performance of combined thermoions system for space nuclear power supply. *Front. Energy Res.* **2020**, *7*, 167. [CrossRef]
2. Moran, M.J.; Shapiro, H.N.; Boettner, D.D.; Bailey, M.B. *Fundamentals of Engineering Thermodynamics*, 9th ed.; John Wiley & Sons Inc.: Hoboken, NJ, USA, 2018.
3. Hu, H.; Liang, S.; Jiang, Y.; Guo, C.; Guo, Y.; Zhu, Y.; Cai, H. Thermodynamic and exergy analysis of 2 MW S-CO_2 Brayton cycle under full/partial load operating conditions. *Energy Convers. Manag.* **2020**, *211*, 112786. [CrossRef]
4. Iverson, B.D.; Conboy, T.M.; Pasch, J.J.; Kruizenga, A.M. Supercritical CO_2 Brayton cycles for solar-thermal energy. *Appl. Energy* **2013**, *111*, 957–970. [CrossRef]
5. Crespi, F.; Gavagnin, G.; S'anchez, D.; Martínez, G.S. Supercritical carbon dioxide cycles for power generation: A review. *Appl. Energy* **2017**, *195*, 152–183. [CrossRef]
6. Al-Sulaiman, F.A.; Atif, M. Performance Comparison of Different Supercritical Carbon Dioxide Brayton Cycles Integrated with a Solar Power Tower. *Energy* **2015**, *82*, 61–71. [CrossRef]
7. Dostal, V. A Supercritical Carbon Dioxide Cycle for Next Generation Nuclear Reactors. Ph.D. Thesis, Czech Technical University in Prague, Prague, Czech Republic, 2004.
8. Marchionni, M.; Bianchi, G.; Tsamos, K.M.; Tassou, S.A. Techno-economic comparison of different cycle architectures for high temperature waste heat to power conversion systems using CO_2 in supercritical phase. *Energy Procedia* **2017**, *123*, 305–312. [CrossRef]
9. Sarkar, J. Second law analysis of supercritical CO_2 recompression Brayton cycle. *Energy* **2009**, *34*, 1172–1178. [CrossRef]
10. Sarkar, J.; Bhattacharyya, S. Optimization of recompression S-CO_2 power cycle with reheating. *Energy Convers. Manag.* **2009**, *50*, 1939–1945. [CrossRef]
11. Wang, J.; Sun, Z.; Dai, Y. Parametric optimization design for supercritical CO_2 pow-er cycle using genetic algorithm and artificial neural network. *Appl. Energy* **2010**, *87*, 1317–1324. [CrossRef]
12. Serrano, I.P.; Linares, J.I.; Cantizano, A.; Moratilla, B.Y. Enhanced arrangement for rec-uperators in supercritical CO_2 Brayton power cycle for energy conversion in fusion reactors. *Fusion Eng. Des.* **2014**, *89*, 1909–1912. [CrossRef]
13. Miao, X.Y.; Zhang, H.C.; Sun, W.B.; Wang, Q.; Zhang, C.X. Optimization of a recompression supercritical nitrous oxide and helium Brayton cycle for space nuclear system. *Energy* **2022**, *242*, 123023. [CrossRef]
14. Sarkar, J. Thermodynamic analyses and optimization of a recompression N_2O Brayton power cycle. *Energy* **2010**, *35*, 3422–3428. [CrossRef]
15. Zhang, X.; Zhang, H.C.; Liu, X.T.; You, E.S.; Yin, D.Z. Performance Analysis and Optimization of a Closed Regenerative Brayton Cycle for Space Nuclear Power System. In Proceedings of the 25th National Academic Conference on Engineering Thermophysics of Colleges and Universities, Roorkee, India, 28–31 December 2019.
16. Wright, S.A.; Pickard, P.S.; Vernon, M.E.; Radel, R.F. Enhancing Power Cycle Efficiency for a Supercritical Brayton Cycle Power System Using Tunable Supercritical Gas Mixtures. U.S. Patent 20130033044 A1, 7 February 2013.
17. Hu, L.; Chen, D.; Huang, Y.; Li, L.; Cao, Y.; Yuan, D.; Wang, J.; Pan, L. Investigation on the performance of the supercritical Brayton cycle with CO_2-based binary mixture as working fluid for an energy transportation system of a nuclear reactor. *Energy* **2015**, *89*, 874–886. [CrossRef]

18. Lemmon, E.W.; Bell, I.H.; Huber, M.L.; Mc Linden, M.O. REFPROP database. In *Reference Fluid Thermodynamic and Transport Properties. NIST Standard Reference Database 23, Version 10.0*; National Institute of Standards and Technology: Gaithersburg, MD, USA, 2013. [CrossRef]
19. Miao, X.Y.; Zhang, H.C.; Zhang, D.; Zhang, C.X.; Huang, Z.L. Properties of Nitrous Oxide and Helium mixtures for space nuclear recompression Brayton cycle. *Energy Rep.* **2022**, *8*, 2480–2489. [CrossRef]
20. Wang, X.R.; Yang, Y.; Zheng, Y.; Dai, Y.P. Exergy and exergoeconomic analyses of a supercritical CO_2 cycle for a cogeneration application. *Energy* **2017**, *119*, 971–982. [CrossRef]
21. Morgon, R. Comparison of High Power Nuclear Systems for Space. In Proceedings of the 18th Intersociety Energy Conversion Conference, Orlando, FL, USA, 21–26 August 1983.
22. Lozano, M.A.; Valero, A. Theory of the exergetic cost. *Energy* **1993**, *18*, 939–960. [CrossRef]
23. Lazzaretto, A.; Tsatsaronis, G. *A General Process-Based Methodology for Exergy Costing*; American Society of Mechanical Engineers: New York, NY, USA, 1996; Volume 36, pp. 413–423.
24. Shokati, N.; Mohammadkhani, F.; Yari, M.; Mahmoudi, S.M.S.; Rosen, M.A. A comparative exergoeconomic analysis of waste heat recovery from a gas turbine-modular helium reactor via organic Rankine cycles. *Sustainability* **2013**, *6*, 2474–2489. [CrossRef]
25. Mohammadkhani, F.; Shokati, N.; Mahmoudi, S.M.S.; Yari, M.; Rosen, M.A. Exergoeconomic assessment and parametric study of a gas turbine-modular helium reactor combined with two organic rankine cycles. *Energy* **2014**, *65*, 533–543. [CrossRef]
26. Khaljani, M.; Saray, R.K.; Bahlouli, K. Comprehensive analysis of energy, exergy and exergo-economic of cogeneration of heat and power in a combined gas turbine and organic rankine cycle. *Energy Convers. Manag.* **2015**, *97*, 154–165. [CrossRef]
27. Bejan, A.; Tsatsaronis, G.; Moran, M. *Thermal Design and Optimization*; John Wiley and Sons Inc.: New York, NY, USA, 1996.
28. Ghaebi, H.; Amidpour, M.; Karimkashi, S.; Rezayan, O. Energy, exergy and thermoeconomic analysis of a combined cooling, heating and power (CCHP) system with gas turbine prime mover. *Int. J. Energy Res.* **2011**, *35*, 697–709. [CrossRef]
29. Misra, R.D.; Sahoo, P.K.; Gupta, A. Thermoeconomic evaluation and optimization of an aqua-ammonia vapour-absorption refrigeration system. *Int. J. Refrig.* **2006**, *29*, 47–59. [CrossRef]
30. Okoro, O.V.; Sun, Z. Desulphurisation of Biogas: A Systematic Qualitative and Economic−Based Quantitative Review of Alternative Strategies. *ChemEngineering* **2019**, *3*, 76. [CrossRef]
31. Ramy, H.M.; Naef, A.A.; Syed, M.Z. Enhancing the thermal and economic performance of supercritical CO_2 plant by waste heat recovery using an ejector refrigeration cycle. *Energy Convers. Manag.* **2020**, *224*, 113340. [CrossRef]
32. Duan, C.J.; Wang, J.; Yang, X.Y. Features of supercritical carbon dioxide Brayton cycle coupled with reactor. *At. Energy Sci. Technol.* **2010**, *44*, 1341–1348.
33. Zhu, Y. Dynamic Analysis of a Closed Brayton Cycle Using Supercritical Carbon Dioxide. *J. Phys. Conf. Ser.* **2021**, *2030*, 012010. [CrossRef]
34. Holland, J.H. An introductory analysis with applications to biology, control and artificial intelligence. In *Adaptation in Nature and Artificial Systems*; MIT Press: Cambridge, MA, USA, 1992. [CrossRef]
35. Yari, M.; Sirousazar, M. A novel recompression S-CO_2 Brayton cycle with pre-cooler exergy utilization. *J. Power Energy* **2010**, *224*, 931. [CrossRef]
36. Lemmon, E.W.; Huber, M.L.; McLinden, M.O. *NIST Standard Reference Database 23: Reference Fluid Thermodynamic and Transport Properties-REFPROP, Version 9.1*; NIST NSRDS; NIST: Gaithersburg, MD, USA, 2010.
37. Akbari Ata, D.; Mahmoudi Seyed, M.S. Thermoeconomic analysis & optimization of the combined supercritical CO_2 (carbon dioxide) recompression Brayton/organic Rankine cycle. *Energy* **2014**, *78*, 501–512. [CrossRef]
38. Zare, V.; Mahmoudi Seyed, M.S.; Yari, M. An exergoeconomic investigation of waste heat recovery from the gas turbine-modular helium reactor (GT-MHR) employing an ammoniaewater power/cooling cycle. *Energy* **2013**, *61*, 397–409. [CrossRef]